Synthesis and Catalytic Activity of Transition Metal Layered Double Hydroxides for OER in Alkaline Medium

A dissertation submitted to the Department of Chemistry , Quaid-i-Azam University, Islamabad, in the partial fulfillment of the requirements for the degree of

Master of Philosophy

in

Physical Chemistry

by

Laiba Jameel

Supervisor

Prof. Dr. Safeer Ahmed

Department of Chemistry
Quaid-i-Azam University,
Islamabad.

2021-2023

بِسْمِ اللَّهِ الرَّحْمَٰنِ الرَّحِيمِ

Al-Quran

"SO surely ease (comes) with every hardship"

"Verily, with (this) hardship (too) there is ease"

94: 5, 6

DECLARATION

This is to certify that this dissertation entitled **" Synthesis and Catalytic Activity of Transition Metal Layered Double Hydroxides for OER in Alkaline Medium"** submitted by ***Ms. Laiba Jameel,*** is accepted in its present form by the Department of Chemistry, Quaid-i-Azam University, Islamabad, as satisfying the dissertation requirements for the degree of ***Master of Philosophy in Physical Chemistry.***

External Examiner:

Prof. Dr. Saima Shabbir
Department of Materials Science and Engineering, Institute of Space Technology, Islamabad.

Supervisor:

04-12-23

Prof. Dr. Safeer Ahmad
Department of Chemistry
Quaid-i-Azam University
Islamabad

Head of Section:

Prof. Dr. Hazrat Hussain
Department of Chemistry
Quaid-i-Azam University
Islamabad.

Chairman:

Prof. Dr. Aamer Saeed Bhatti (TI)
Department of Chemistry
Quaid-i-Azam University
Islamabad

DEDICATION

Dedicated to my loving parents,

Mr. and Mrs. Jameel Ahmad,

my supervisor **Prof. Dr. Safeer Ahmed,**

my teachers and siblings.

Thanks for your support and prayers.

Acknowledgements

All glory and praise belong to **Allah Almighty** ,the most Compassionate and Merciful, who blessed me with an opportunity for M.Phil. studies and providing the strength to overcome all challenges encountered during the completion of this research work. I confirm my conviction that the **Holy Prophet Muhammad (P.B.U.H)** is the messenger of Allah, and his life stands as an impeccable model for all of humanity, guiding us until the day of judgment.

It brings me great joy to express my sincere thanks to my supportive, inspiring, and esteemed supervisor, **Prof. Dr. Safeer Ahmed**, for entrusting me with the opportunity to conduct research under his guidance. I would also like to express my sincere gratitude to **Prof. Dr. Aamer Saeed Bhatti (**Chairman of the Department of Chemistry) and **Prof. Dr. Hazrat Hussain** (Head of the Physical Section) for granting me access to the laboratory facilities. I express my gratitude to all my respected teachers for their guidance and inspiration.

I am so blessed to have such loving and supportive **parents,** who have always been there for me, cheering me on every step of the way. I am thankful to my **siblings,** without their moral support , perhaps this research might not have seen the light of the day. I am grateful to my seniors and fellows **(Rida Batool, Abdul Karim, Atiqa Jabeen, Javaria Idrees, Afifa Irfan and Syeda Kainat Fatima)** always being there for me to help and cooperate whenever I needed assistance during my research work. I would like to thanks all my friends and lab fellows **(Saba, Alizay, Hafsa, Amna Aneesa, Arooj and Ahsan)** for their help and support throughout the whole journey. I pray that Allah continues to bless and guide us all in our endeavors.

Laiba Jameel

Table of Contents

List of Figures

List of Tables

List of Abbreviations

CoFe-LDH	CoFe-Layered double hydroxides
CoFe-LDH/rGO	CoFe-Layered double hydroxides/reduced graphene oxide
CV	Cyclic voltammetry
CNT	Carbon nanotube
EIS	Electrochemical impedance spectroscopy
GO	Graphene oxide
GCE	Glassy carbon electrode
HMT	Hexamethylenetetramine
HER	Hydrogen evolution reaction
ICDD	International center for diffraction data
JCPDS	Joint committee on powder diffraction standards
LDH	Layered double hydroxides
LSV	Linear sweep voltammetry
NiCo-LDH	NiCo-layered double hydroxides
NiCo-LDH/rGo	NiCo-layered double hydroxides/reduced graphene oxide
NiFe-LDH/rGO	NiFe-layered double hydroxides/reduced graphene oxide
NiFe-LDH	NiFe-layered double hydroxide
ORR	Oxygen reduction reaction
OER	Oxygen evolution reaction

rGO	Reduced graphene oxide
RHE	Reversible hydrogen electrode
MWCNT	Multi walled carbon nanotubes
TM-LDH	Transition metal based layered double hydroxides
TM-LDH/rGO	Transition metal based layered double hydroxides/reduced graphene oxide
TMPs	Transition metal phosphides
XRD	X-ray diffraction

Abstract

Electrochemical water splitting has been empirically proven to be a potential technology for hydrogen generation. Hydrogen is a promising candidate in the context of energy conversion and storage application. The oxygen evolution reaction (OER) which demands a large overpotential, stands out as the most crucial process among the various stages involved in water electrolysis. Addressing this challenge primarily involves developing OER electrocatalysts that are efficient, long-lasting, environmentally friendly, and cost-effective. The objective of present research work was to fabricate transition metal-based layered double hydroxides (TM-LDHs), and their composites with rGO (TM-LDH/rGO), to study their OER performance. Different TM-LDH materials (NiFe-LDH, NiCo-LDH, CoFe-LDH, NiFe-LDH/rGO, NiCo-LDH/rGO and CoFe-LDH/rGO) were successfully synthesized by hydrothermal method and confirmed by XRD and FTIR analyses. The OER activity of synthesized electrocatalysts was systematically evaluated in an alkaline medium by employing linear sweep voltammetry (LSV), cyclic voltammetry (CV), and electrochemical impedance spectroscopy (EIS) techniques using glassy carbon (GC) as substrate. The CV scans displayed the characteristic redox behavior related to each modified electrode. The OER performance of all synthesized electrocatalysts was compared in terms of overpotential at 10 mA cm^{-2} and the Tafel slope, which declines in the order NiFe-LDH/rGO (260 mV, 46.4 mV dec^{-1}) > NiFe-LDH (270 mV, 51.5 mV dec^{-1}) for Ni-Fe combination, CoFe-LDH/rGO (310 mV, 53.4 mV dec^{-1}) > CoFe-LDH (330 mV, 80.6 mV dec^{-1}) for Co-Fe combination of LDH and NiCo-LDH/rGO (320 mV, 77 mV dec^{-1}) > NiCo-LDH (390 mV, 77 mV dec^{-1}) for Ni-Co combination of LDH. Among all the synthesized electrocatalysts, NiFe-LDH/rGO exhibited the highest OER activity with an overpotential of 260 mV.

CHAPTER 1

INTRODUCTION

There is a critical need to investigate clean energy resources to replace conventional fossil fuels due to the growth in environmental challenges and sustainable energy requirements in the 21st century. Due to its significant gravimetric energy density, absence of carbon dioxide emissions, and eco-friendliness, hydrogen (H_2) has recently been considered a useful energy source [1]. To create a stable and economically viable hydrogen economy, it is necessary to reduce the expense of sustainable hydrogen production by water electrolysis. Therefore, it is essential to develop economical and stable catalysts for the electrolysis of water [2]. Furthermore, by utilizing modern electrocatalytic water splitting methods, renewable energy may be efficiently changed into more precious hydrogen energy, enhancing the diversity of sustainable energy consumption [3].

1.1 Electrochemical water splitting

Water splitting is a procedure in which water breaks down into its primary components, oxygen, and hydrogen. In 1789, van Trostwijk and Deiman made initial observations regarding the electrolysis of water, marking the inception of this significant scientific advancement [4].

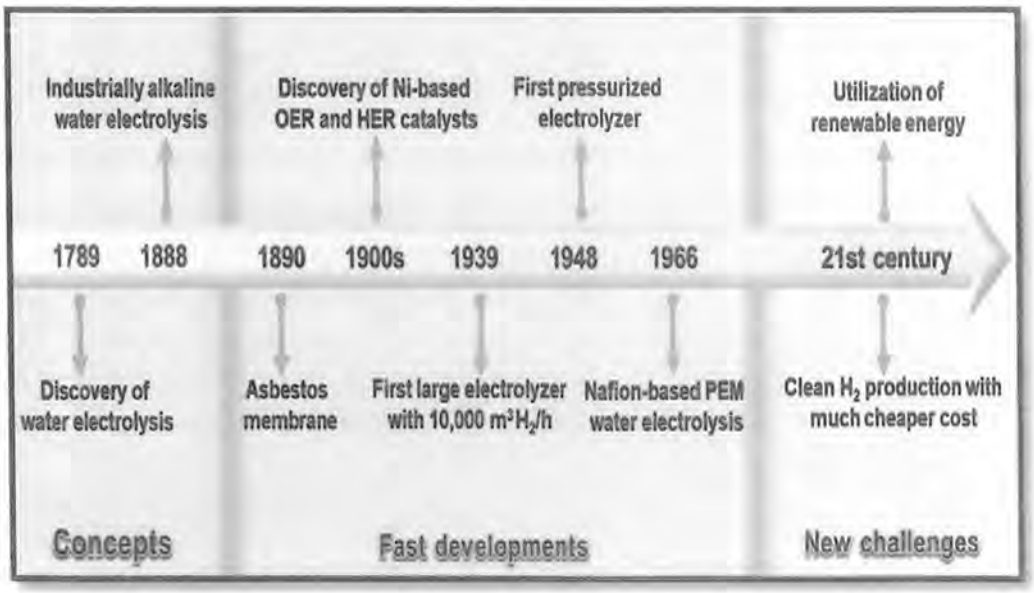

Fig. 1.1 The advancements in water electrolysis [5].

Since its first discovery, over 200 years have passed in the history of water electrolysis. Three separate stages in the development of electrocatalysis include the discovery of process, the explosive expansion of industrial water electrolysis, and the present day application of renewable energy to manufacture inexpensive hydrogen. **Fig. 1.1** provides a concise overview of noteworthy events and key milestones in developmental history of water electrolysis [5].

The reaction for overall water splitting is given in **equation 1.1** :

$$2H_2O_{(l)} \rightarrow O_{2(g)} + 2H_{2(g)} \qquad E = 1.23 \text{ V vs. (RHE)} \qquad \textbf{(1.1)}$$

Electrochemical water splitting takes place when an external voltage is supplied across the cell. The water electrolysis process consists of two half-reactions carried out at cathode and anode are identified as hydrogen evolution reaction (HER) and the oxygen evolution reaction (OER) , respectively. When an electrical current flows through H_2O, hydrogen is generated at the cathode by reducing water, while oxygen is generated at the anode by oxidization of water [6].

Electrochemical water splitting uses low-cost water as a starting material to manufacture hydrogen that is highly pure at ambient temperature without any greenhouse emissions [7]. However, this approach has significant challenges, such as poor efficiencies and high overpotential due to slow four proton-coupled kinetics in OER and relatively large over-potential for HER. Thus, both OER and HER demand effective and stable electrocatalysts to increase the kinetics of used in practical hydrogen generation [8].

1.1.1 Oxygen evolution reaction

Water oxidation (or hydroxyl ions in a basic medium) takes place at a positively charged electrode (anode) to form oxygen gas by the release of electrons. A four-electron transfer process occurs stepwise to produce one oxygen molecule. The overall reaction for OER is shown in **equation 1.2** (in basic medium) and **equation 1.3** (in acidic medium).

Basic medium $4OH^-_{(aq)} \rightarrow O_{2(g)} + 2H_2O_{(l)} + 4\,e^-$ $E^o = 0.40$ V vs.(RHE) **(1.2)**

Acidic medium $2H_2O_{(l)} \rightarrow 4H^+_{(aq)} + O_{2(g)} + 4\,e^-$ $E^o = 1.23$ V vs.(RHE) **(1.3)**

The hydroxyl ion-rich alkaline medium has a higher rate of water oxidation at the anode side than an acidic medium. However, the restricted current density hinders the potential for achieving higher performance and broader practical utility [9, 10].

1.1.2 Hydrogen evolution reaction (HER)

At cathode, which is a negatively charged electrode, hydrogen ions (or water in an alkaline medium) are reduced to produce hydrogen gas. This process involves a stepwise reaction of two-electron transfers to yield one mole of hydrogen gas. For the production of hydrogen, HER has been thoroughly examined for almost all transition metals [9, 11].The overall reaction for HER is shown in **equation 1.4** (in basic medium) and **equation 1.5** (in acidic medium).

Basic medium $4H_2O_{(l)} + 4\,e^- \rightarrow 4OH^-_{(aq)} + 2H_2$ $E^o = -0.83$ V vs. (RHE) **(1.4)**

Acidic medium $4H^+_{(aq)} + 4\,e^- \rightarrow 2H_{2(g)}$ $E^o = 0.00$ V vs. (RHE) **(1.5)**

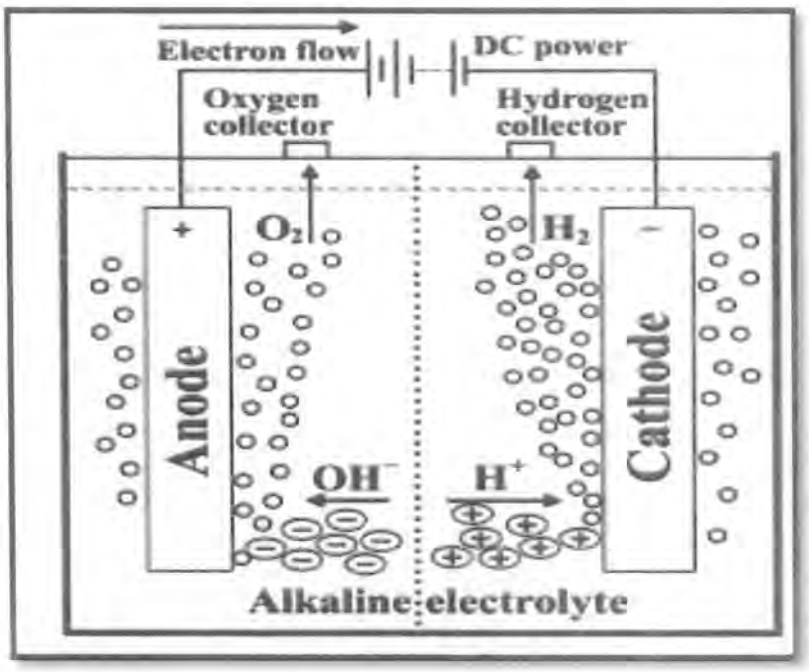

Fig. 1.2 A basic schematic representation of a simple alkaline water electrolysis system [13].

The activity of HER is higher in acidic media(low-pH) as compared to in basic medium (high-PH). This is mostly because the reaction is restricted by the slow water dissociation step. But on a commercial scale, alkaline electrolysis is preferable [12].

1.1.3 Kinetics and thermodynamics

OER occurs at interface of electrode-electrolyte in which includes three different phases: solid (catalyst), liquid (water) and gaseous (oxygen). Three main stages that are typically involved in the evolution of oxygen are as follows:

1) Adsorption of hydroxyl ions or water molecules onto the electrocatalyst's active sites.

2) Simultaneous transfer of protons and electrons.

3) Rearrangement of configuration to allow O_2 to be released from the surface of catalyst and disperse into electrolyte [14].

Furthermore, for industrial electrolyzers, water electrolysis occurs at a significant cell potential from 1.8 V to 2.0 V , which is greater (0.55-0.77 V) than its theoretical value (1.23 V) under standard conditions (25 °C and 1atm) [15]. The word "**overpotential**" refers to this extra potential necessary to break through the reaction system's energy barrier. This overpotential may be due to several reasons such as the activation barrier at the anode, resistance between electrolyte and electrode , circuit resistance, kinetic limitations of OER having a sluggish four-electron transfer process and the relatively easier reduction involving two-electron process HER etc. As a result, practically, the water splitting requires a potential more than theoretical thermodynamic potential. This overpotential can be reduced by using effective, long-lasting, and environmentally friendly electrocatalysts for HER and OER. Additionally, by improvement in the design of electrolyzer, additional causes producing resistance can be addressed. This method helps to make electrochemical water splitting more ecologically friendly and cost-effective [16, 17].

However the loss of energy for OER is much greater than that for HER due to its sluggish kinetics which is why OER has been referred to as a bottleneck reaction [14].At 25 °C, the standard potential (E°) required for water electrolysis is 1.23 V, and the

corresponding change in Gibbs free energy for reaction is 237.2 kJ/mol. This is according to equation that relates equilibrium cell voltage with change in Gibbs free energy ΔG as shown in **equation 1.6**.

$$\Delta G^{\circ} = n\,FE^{\circ} \qquad (1.6)$$

Here n represents the number of moles of electron that transferred during the reaction (each mole of water needs two moles of electron), E° is equilibrium cell voltage and F shows the Faraday constant value indicating charge on one mole of electrons that is 96485 C/mol. This is an ideal case, but additional energy is also needed to control the entropy shift of the reaction. As a result, in the absence of external heat/energy, the process cannot proceed below 286 kJ per mol [18].

1.2 Electrocatalyst

Many types of electrocatalysts are being used in water-splitting reactions to decrease the overpotential for both HER and OER.

1.2.1 Working

Electrocatalysts work at the electrode surface or can even be at the electrode surface [19]. The non-negative value of Gibbs free energy indicates that water electrolysis is not just an uphill reaction but requires overcoming a significant kinetic barrier.

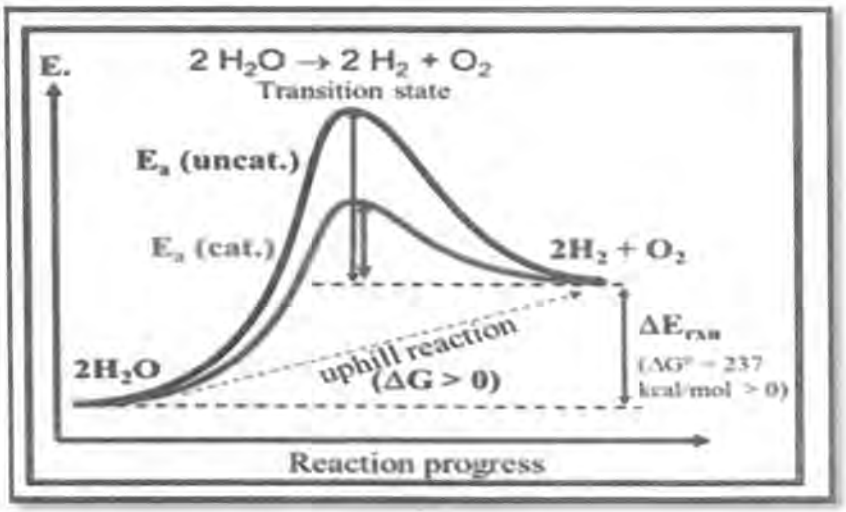

Fig. 1.3 Schematic illustration showing the role of catalyst in decreasing the activation energy barrier [20].

Electrocatalysts are essential for decreasing the kinetic barrier without being consumed (**Fig. 1.3**) [20]. An electrocatalyst facilitates specific chemical interactions or can increase the rate at which electric charge is transferred at the surface of the electrode [21].

1.2.2 Properties

The assessment of an electrocatalyst's performance involves various critical characteristics such as activity, stability, selectivity, and efficiency [20]. In water electrolysis, the catalyst's structure plays a crucial role in achieving efficient performance. An optimal electrocatalyst structure should provide a broad active surface area, effective pathways for gas release, proficient electron conduction, and prevent excessive clustering [22].

1.2.3 Some general examples of electrocatalysts

Costly metal oxide (IrO_2 and RuO_2) and Pt-involved systems are often considered the most efficient benchmark electrocatalysts in acidic environments with low Tafel slope, lower overpotential, extended strength, and large value of exchange current density for OER and HER, respectively [23, 24]. But there are two issues: (1) high cost and limited availability; and (2) dissolution, catalyst poisoning during electrocatalysis and agglomeration, due to these issues the practical use of water electrolysis over these precious metal-based electrocatalysts is not captivating. Huge efforts have been taken to build affordable and efficient transition metal-based catalysts for both OER and HER (that work in alkaline medium) which might be the ideal replacement for these expensive and poorly stable electrocatalysts in the awareness of a hydrogen-based economy [25, 26]. In recent times compounds based on first-row transition metal (Cu, V, Co, Ni, Ti, Mn, Cr, Zn, Fe), such as phosphides, nitride, hydroxides, oxides, sulfides, and selenides have been recognized as the most effective OER and HER candidates [3, 27].

1.3 Electrocatalyst materials for OER

1.3.1 Transition metal hydroxides

Innovative commercial catalysts like RuO_2 and IrO_2 display exceptional catalytic performance for the OER. Nevertheless, this kind of catalyst depending on precious metals, are susceptible to instability when exposed to high anodic potentials in alkaline electrolytes this instability leads to the generation of RuO_4 and IrO_3 respectively, which can gradually

dissolve in the solution. Furthermore, the constrained accessibility and significant expense of these catalysts based on noble metals, complicate their practical application [28, 29]. Hydroxides based on transition metals (like Fe, Mn, Ni and Co) have been extensively studied and shown promising OER performance. Among these active electrocatalysts for OER, 2D layered double hydroxides (LDHs) based on transition metals have been considered among the most promising materials because of their distinctive structural composition, physicochemical characteristics, synthesis methods, and better catalytic activity. These advantages have attracted significant research attention in using LDHs as electrocatalyst for OER [29].

1.3.2 Transition metal oxide families

Transition metal-based oxides including spinal oxides, perovskites and amorphous metal oxides have been discovered to show good catalytic activity for OER.

- **Spinel family**: Transition-metal oxides having spinel structures, like Co_3O_4, and MnO_2, have been extensively studied for their use in OER. These spinel oxides are part of a larger group known as AB_2O_4, which includes cation A, which normally has a +2 charge and is found in tetrahedral positions, and cation B, which typically has a +3 charge and is found in octahedral positions. Spinel oxides are classified as either normal or inverse spinel structures based on how cations are distributed throughout the tetrahedral and octahedral positions. Spinel oxides are known for their exceptional OER capacity, attributed to their wide range of compositions, differing valence states, and the synergistic effects they exhibit. The majority of OER electrocatalysts derived from spinel oxides are primarily composed of cobalt-based and iron-based (ferrite) compounds, often doped with various transition and alkaline metals like Mn, Ni, Cu, Zn, and Li [14, 30].
- **Perovskite oxide**: Perovskites belong to a category of materials characterized by a general chemical formula, ABO_3. Site A in this formula can be filled by either an alkaline or a rare-earth metal atom. The transition metal atom, indicated as B, is in the core of an octahedron, and these octahedra are joined at their corners. Site A can fill empty gaps, assisting in the creation of the perovskite structure. Depending on the oxidation state of atom A, the oxidation state of the transition metal (B) in perovskites

can be +3, +4, or a combination of both. The elemental composition of perovskite materials is highly adaptable, with the potential to incorporate over 90% of metallic elements to synthesize various perovskite families [14, 31]. According to Bockris and Otagawa's complete OER investigation based on a perovskite family, OER activity for several transition metals in perovskites follows a pattern (Ni > Co > Fe > Mn > Cr) [32].

- **Amorphous transition-metal oxide**: Recently, amorphous metal oxides have emerged as promising candidates for catalyzing OER. A significant portion of surface-exposed defects are derived from short-range ordered structures and these defects function as catalytically active sites. Furthermore, amorphous phases offer distinct advantages in terms of both mechanical and electrochemical stability, which has stimulated extensive research into amorphous metal oxide catalysts. Approximately 20 distinct amorphous complex metal oxide films, incorporating iron, nickel, and cobalt have been fabricated and assessed for their performance in OER. Remarkably, the a-$Fe_{20}Ni_{80}$ film emerged as the most promising candidate. Notably, even minute additions of iron can impact Tafel slopes, while the inclusion of nickel or cobalt can effectively reduce the voltage required for catalytic initiation [33].

1.3.3 Transition metal based non-oxide electrocatalyst

Non-oxides based on transition metal are also used as electrocatalyst both OER and HER. These includes transition metal-based sulfides and phosphides etc.

- **Transition metal phosphides**: Transition metal phosphides (TMPs) have attracted a lot of research interest due to their abundance in the Earth's crust and catalytic properties comparable to those of noble metals. TMPs formed by six distinct transition metals (Fe, Co, Ni, Cu, Mo, and W) have been discovered to be useful in electrochemical hydrogen evolution [34, 35] .

The catalytic activity of TMP catalysts in water splitting is primarily attributed to the suitable surfaces for proton and hydride acceptance, which facilitate moderate bonding between the phosphorus within the catalyst's structure and reaction intermediates [36]. Electrocatalysts containing cobalt-based phosphides, such as Co_2P, CoP, CoP_2, and CoP_3 have been extensively investigated for their ability to serve as

bifunctional electrocatalysts for HER and the oxygen evolution reaction OER. This is because of their exceptional electrical conductivity and strong durability, which holds in both acidic and alkaline environments [8, 37].

- **Transition metal-based sulfides:** Bifunctional electrocatalysts based on transition metal sulfide nanomaterials have a lot of potential because of their distinctive construction and significant concentration of defect locations [38]. Different phases of cobalt sulfides, including Co_9S_8, Co_3S_4, and $Co_{1-x}S$, have been explored OER catalysts [39]. Ni-based sulfide electrocatalysts have also been thoroughly researched as inexpensive HER and OER catalysts [8].

1.4 Layered double hydroxides

Layered double hydroxides (LDHs), commonly referred to as anionic clays, known as materials having to resemblance to hydrotalcite, constitute a diverse category of 2D materials. They consist of layers of positively charged hydroxides with negatively charged anion in interlayer spaces. Hydrotalcite structures are notably robust and offer considerable versatility in terms of potential compositions and readily adjustable functional properties [40]. This particular lamellar ionic material consists of positively charged layers resembling brucite. These layers contain both trivalent and divalent metal cations, while the interlayer charge is balanced by inorganic/organic anions and water molecules.

The structure of LDH is represented by general formula $\mathbf{[M_{1-x}^{2+} M_x^{3+}(OH)_2]^{x+}[A_{x/n}]^{n-}.mH_2O}$ where M^{3+} (Fe^{3+}, Tb^{3+} Al^{3+}, Co^{3+}, Cr^{3+}, , Mn^{3+} , V^{3+} and Ga^{3+}) and M^{2+} (Pd^{2+}, Mn^{2+}, Ca^{2+}, and Cd^{2+} Mg^{2+}, Ni^{2+}, Co^{2+}, Zn^{2+}, Cu^{2+}) are trivalent and divalent metal cations respectively, 'A' represents the anion (CO_3^{2-}, NO_3^-, RCO_2^-, VO_4^{3-}, SO_4^{2-}, Cl^- and MoO_4^{2-} etc.) that reside in between the interlamellar space metal hydroxide layer containing positive charge, 'n' represents the charge carried by interlayer anions, while 'm' denotes the water content.. Furthermore, 'x' represents the molar ratio of trivalent metal cation to the total metal cations, expressed as $x = M^{3+}/M^{2+} + M^{3+}$.This ratio falls within the range of $0.2 \leq x \leq 0.33$. The fundamental structure of LDH is similar to hydrotalcite compounds found in nature, which are composed of Al^{3+} and Mg^{2+} metal cations having chemical formula $Mg_6Al_2.(OH)_{16}.CO_3.4H_2O$ [3].

The layers can be layered either with a hexagonal cell (2H) or rhombohedral (3R) structure. The 2H homolog is known as manasseite, and hydrotalcite has the 3R symmetry [41]. **Fig. (1.4)** shows the characteristic layered structure of LDH.

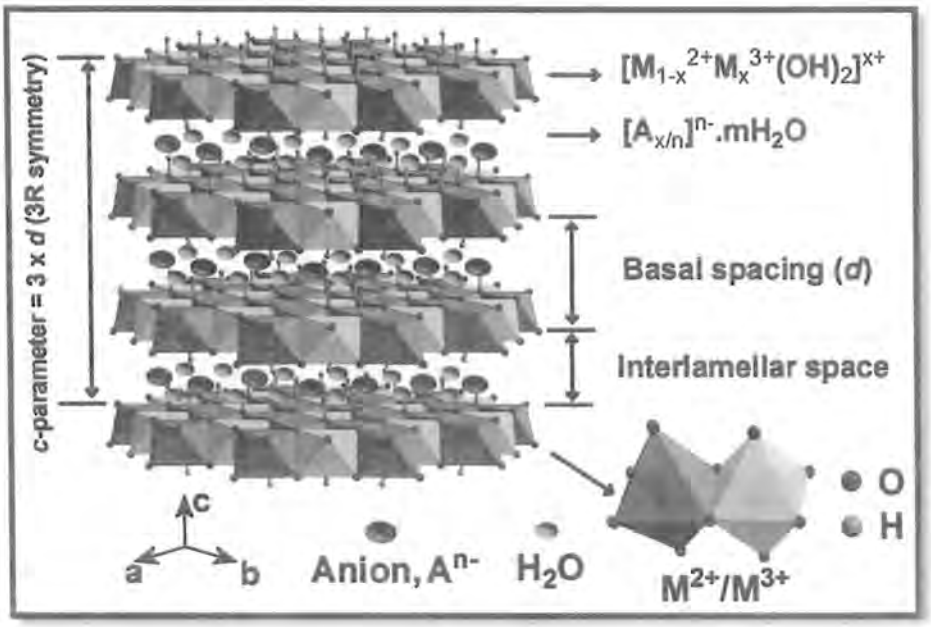

Fig. 1.4 Visual representation that depicts the layered structure of LDH. [Rhombohedral (3R-symmetry) corresponds to hydrotalcite] [41].

1.5 Properties of LDHs

- LDHs' characteristic 2D layered design provides various advantages:
  - (i) It enables adjustable modification of metal cations inside the bulk layer.
  - (ii) It allows for the interchange of different interlayer anions while keeping control over interlayer spacing.
  - (iii) With the help of external driving forces, such as a simple ultrasonication technique, it becomes simple to increase the interlayer gaps and even exfoliate bulk LDHs into incredibly thin nanosheets [42].
- M^{2+} ions undergo isomorphism and are replaced by M^{3+} cations within the layers of brucite. These layers are made up of edge connecting (M^{3+}, M^{2+}) $(OH)_6$ Octahedral units that form continuous layers, featuring -OH bonds, aligned vertically along the planes. Furthermore, due M^{2+} and M^{3+} metal cations within MO_6 octahedral unit of brucite layer gives the metal hydroxide frameworks a positive charge. The degree of

positional arrangement of M^{3+} and M^{2+} ions within the hydroxide layer may differ based on the specific cation type involved.

- Cohesive force arises among the brucite layers because of:
  - (i) H-bonding in between and O-atoms of interlayer anion and brucite layers of -OH groups, governed by co-ordination equilibrium .
  - (ii) The electrostatic attraction that arises between negatively charged interlayer species M-OH sheets containing positive charge [3].
- LDHs are ionic solids by nature so they have less issues related to ionic conductivity, they are efficient materials to use in electrochemical research, such as the OER process, and have enhanced OER performance.
- When LDH materials are subjected to a blend of stereoisomers and enantiomers of crucial organic compounds used in industry, such as benzene-dicarboxylates and p-nitro phenol, they exhibit selective behavior in exchanging the interlayer species. As a result, it also aids in the purification of organic molecules and in raising the enantiomeric excess of various fine chemicals [43].

1.6 Transition metal based LDH (TM-LDH)

TM-LDH is a type of LDH material having positively charged layers composed of transition metal cations in their characteristic layered structure. TM-LDH have been the subject of extensive research recently and shown to exhibit exceptional performance as electrocatalysts for OER due to the following characteristics:

- Their affordable accessibility and the flexibility of chemical compositions within the layered structure containing positively charged multi-transition-metal cations and charge-balancing interspace anions and H_2O molecule [44].
- As compared to single metal hydroxides, TM-LDH exhibit the ability to accommodate a wide range of electron carriers, inorganic and organic anions, and can undergo orbital transformations to enhance their activity performance in OER, surpassing that of single metal hydroxides. tolerate. In TM-LDH the homogenous dispersion of trivalent and bivalent metallic ions serve as active electrocatalytic sites that lead to good OER efficacy [44].

- 3D transition metal-based LDH are promising and trending OER electrocatalyst. In the case of TM-LDH, a variety of combinations for divalent and trivalent like Co-Fe, Ni-Co, Mn-Fe, Mn-Fe, Ni-V, Co-Cr, Ni-Fe and Ni-Mn are identified as suitable electrocatalysts suitable for OER in basic medium. The presence of at least one among the three iron group metals (Co, Fe and Ni) is observed in those TM-LDH materials that are being applied as OER Catalyst. This means that, while several combinations of TM-LDH are conceivable, the main condition is that it should have a layered structure with the existence of any among these three iron group metals, preferably as divalent metal cation in hydroxide layers, show good OER activity [43, 45-47].

1.6.1 NiFe-LDH

In this combination of TM- LDH the nickel and iron present in bivalent and trivalent states respectively and having the general chemical formula $[Ni(II)_{1-x}Fe(III)_x(OH)_2]^{x+}(A^{n-})_{x/n}\cdot yH_2O$, where, 'A' is an intercalated anion, 'x' indicates the molar ratio of Fe in NiFe-LDHs n is the charge of the anions and y represent water content between layers. It is widely understood and well-reported that NiFe-LDH exhibits excellent electrocatalytic performance for the OER in basic conditions due to the following features

- A balanced push-pull sequence arises between the Fe and Ni metal centers, effectively distributing electron density and enabling the entry of OH ions that start the reaction [48].
- NiFe LDHs exhibit notably lower Tafel slopes and overpotential (η) values in comparison to various alternatives within the LDH family and other metal oxides currently under examination for OER. This can be attributed to the presence of numerous highly active sites in proximity to the edges of the platelets [49-51].
- $Ni(OH)_2$ and NiOOH exhibit limited effectiveness as OER electrocatalysts. Consequently, there is a significant drive to investigate the OER performance of iron-based LDH, as it is crucial for comprehending the enhanced activity of NiFe-LDH and has generated substantial interest. and NiOOH are not as effective as OER electrocatalysts [52].
- During their investigation, Friebel and Bell examined the intrinsic OER performance of γ-FeOOH. They observed that it displayed a lower overpotential of 550 mV@10 mA

cm^{-2} in a 0.1 M KOH solution compared to Fe-free NiOOH, which had an overpotential (η) of 660 mV at the same current density and electrolyte. However, this overpotential was considerably higher than that of (Ni, Fe) OOH, which exhibited an overpotential of 360 mV at 10 mA cm^{-2} in 0.1 M KOH [53].

- The crystallographic phases of $Ni(OH)_2$-based catalysts reveal the presence of two dehydrated phases, namely β-NiOOH and β-$Ni(OH)_2$, as well as two hydrated phases, NiOOH and α-$Ni(OH)_2$. Trotochaud et al. have demonstrated that when Fe^{3+} is partially included as metal centers in the hydroxide structure, as observed in the case of NiFe-LDH, it narrows down the phasing scheme to only the hydrated α and ɣ phases. These structural transitions are known to enhance specific material properties, such as packing density and crystal order, resulting in heightened electrocatalytic activity [54,55]. Both practical experiments and theoretical research in the literature have validated these enhancements.

  Furthermore, given that potassium hydroxide is frequently used as an alkaline electrolyte, it's worth noting that the layer contraction, primarily indicating a phase change, is followed by the intercalation of metal cations, typically K^+ ions. Hence, the increased performance (in Ni-Fe based system) is mostly attributable to the structure's layer contraction and increase in crystallinity, which both boost conductivity and, in turn, the system's capacity to catalyze reactions at greater rates [48].

1.6.2 CoFe-LDH

In of CoFe-LDH the cobalt and iron present in bivalent and trivalent states respectively in its layered characteristic structure and having the chemical formula $\mathbf{[Co(II)_{1-x}Fe(III)_x(OH)_2]^{x+}(A^{n-})_{x/n}\cdot yH_2O}$.In this context, x denotes the molar ratio of Fe^{3+} in CoFe-LDHs, 'A' represents an intercalated anion, 'n' corresponds to the charge carried by the interlayer compensating anions, and 'y' signifies the quantity of water present between the layers [56]. For CoFe-LDH, it was discovered that the activity of OER was significantly improved by Fe inclusion over pure cobalt compounds [57].

- CoFe-LDH, similar in structure to hydrotalcite, offers a substantial quantity of active sites that facilitate efficient OER due to their permeability to electrolytes. Additionally,

iron (Fe) exhibits the highest intrinsic activity and can function as dynamically active sites within the CoO_xH_y host [56].

- The enhancement of OER is driven by favorable interactions between the Fe and Co sites. Hung et al. observed that during OER, Fe stabilizes Co ions at a higher oxidation state, which in turn promotes the generation of more resilient reactive intermediates [58].
- CoFe-LDH serves as a substitution for cobalt in the octahedral arrangement of cobalt hydroxides. This substitution leads to a positive charge on the layers in $Co(OH)_2$. To balance these positively charged layers, anions like CO_3^{2-}, SO_4^{2-}, Cl^- and NO_3^- intercalate into the interlayer region of cobalt hydroxides. Therefore, $Co(OH)_2$ can be used as a model to examine their crystalline structures.
- Cobalt hydroxides exhibit two primary crystallographic phases: stoichiometric β-$Co(OH)_2$ and isostructural α-$Co(OH)_2$. The α-$Co(OH)_2$ phase is metastable and consists of positively charged $Co(OH)_{2-x}$ layers with intercalated anions in the interlayer space to maintain charge neutrality. This phase readily transforms into β-$Co(OH)_2$.

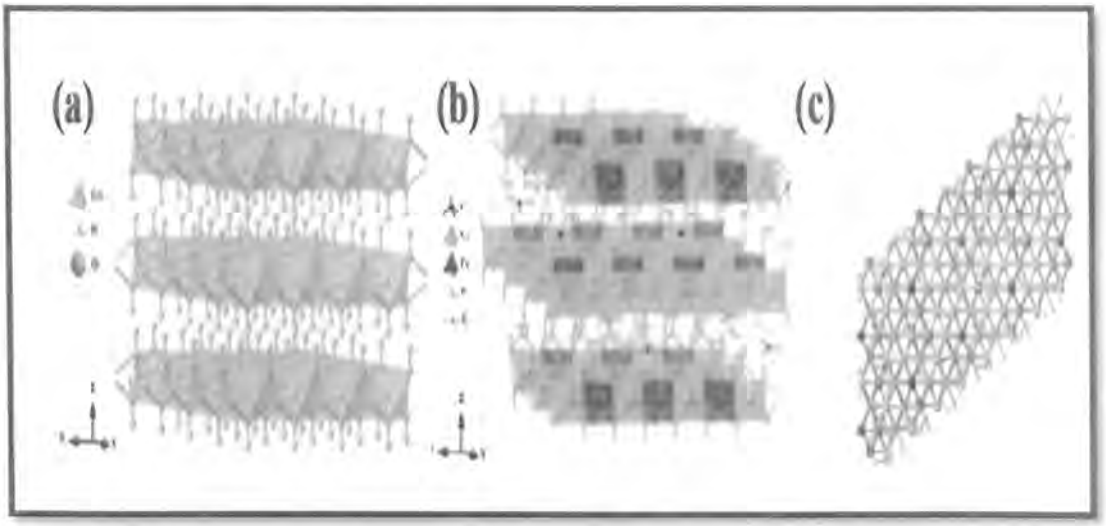

Fig. 1.5 Optimal structure for **(a)** β-$Co(OH)_2$ and **(b)** CoFe LDH (having Co/Fe = 3/1) extending along the c-axis in the crystallographic dimension, with randomly distributed interlayer carbonate anions and water. (c) Top view of CoFe LDH in the direction of c-axis [56].

In contrast, β-$Co(OH)_2$ consists of hexagonally arranged hydroxyl ions, with bivalent cobalt ions occupying alternating rows of octahedral sites as shown in **Fig. 1.5.** Additionally, Van der Waals forces act between layers in β-$Co(OH)_2$, similar to other layered materials like MoS_2 and graphite. The β-$Co(OH)_2$ structure resembles that of brucite, featuring a hexagonal lattice with trigonal crystal symmetry in the P-3m1 space group [29, 56, 59].

- Based on density functional theory (DFT) calculations, a synergistic effect of Fe and Co in CoFe LDHs for water oxidation is proposed, which is responsible for their enhanced OER activity. According to Dionigi et al., single Fe sites and pure Co-Co centers are less effective for stabilizing intermediate of OER as compared to surface Fe sites that synergize with nearest-neighbor Co sites via O-bridged Fe-Co reaction sites [60].

1.6.3 NiCo-LDH

NiCo-LDH represents the general formula $[Ni(II)_{1-x}Co(II)_x(OH)_2]^{x+}(A^{n-})_{x/n}\cdot yH_2O$, In this context, 'x' signifies the molar ratio of cobalt in CoFe-LDHs, 'A' represents intercalated anions, 'n' denotes the charge carried by the anions, and 'y' indicates the quantity of water situated between the layers. The following features show that NiCo-LDH can also be used:

- Single nickel hydroxide-based materials show poor have poor contact among active ions so because of synergistic effect between cobalt and nickel, incorporation of cobalt can amplify its electrical conductivity of electrode material. materials hence improving OER performance [61].
- X-ray photoelectron spectroscopy (XPS) was employed to assess the chemical states of the synthesized NiCo-LDH materials by Ar plasma at various periods. After being bombarded by plasma, the peaks of Ni and Co change to have lower binding energies, suggesting that Co and Ni have undergone higher oxidation states [62].
- These higher oxidation states may facilitate charge transfer at the electrode-electrolyte interface and improve electrolyte diffusion, which may be advantageous for electrocatalytic processes. Simultaneously, the greater density of these higher states facilitates OER [62, 63].

- NiCo-LDH nanosheets have Co and Ni in various valence states shown by XPS analysis. So, it is quite reasonable to anticipate that the solid-state redox pairs involving Ni^{2+}/Ni^{3+} and Co^{2+}/Co^{3+} within NiCo-LDH nanosheets could yield significant electrochemical performance improvements. This is due to the recognition of Ni^{3+} and Co^{3+} cations as the catalytically active sites for OER [64] .

1.7 General mechanism of OER on TM-LDH surface

On the surface of LDH (M), several electron-transfer stages, including those involved in the mechanism of OER in both alkaline and acidic mediums are depicted in **Fig. 1.6**. This sequential electron-transfer phenomenon is named the Adsorbate evolution mechanism (AEM). This series of electron transfers that take place as part of LDH for the OER process in both acidic and basic medium are known as the adsorbate evolution mechanism (AEM) [3, 44].

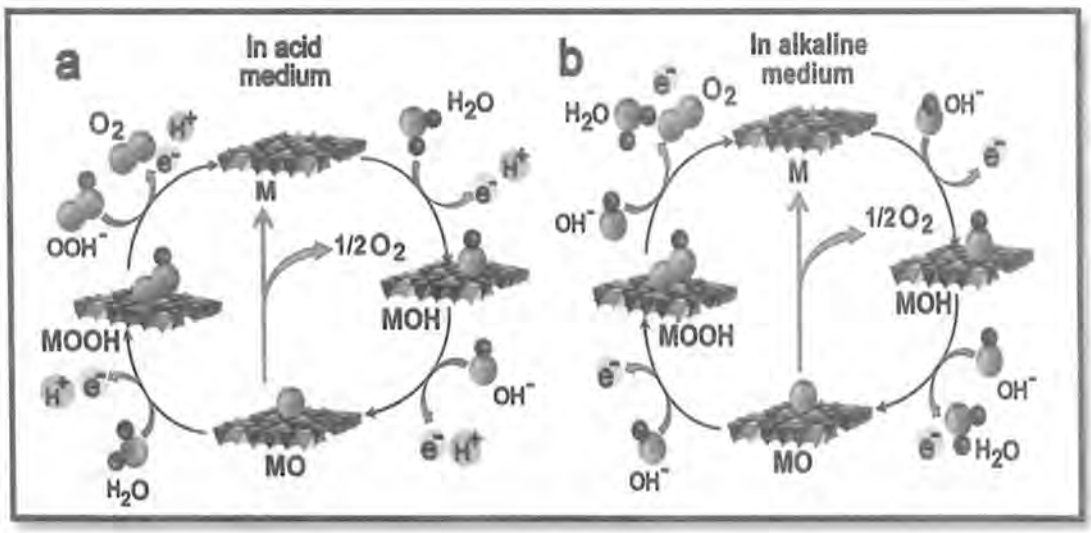

Fig. 1.6 OER mechanism on TM-LDH [Adsorbate evolution mechanism (AEM)] **(a)** in acidic medium **(b)** in basic medium [44].

Although metal components are frequently used as the active site in OER, understanding the OER procedure is necessary when building TM-LDH for OER. The kinetic barrier that arises during the OER can be significantly overpowered by the sluggish kinetics of O-O covalent bonding. In both acidic and alkaline environments, O_2 is produced from MO intermediates in two different pathways. In acidic medium, the combination of

MO and water results in the formation of MOOH, which subsequently breaks down to produce oxygen. Additionally, it is quite likely that MO encourages efficient O_2 generation. However, in an alkaline medium, the successful generation of oxygen occurs by both the fragmentation of MO and the interaction of newly produced M-OOH with -OH. The complete effectiveness of the TM-LDH towards OER is further determined by the intermediate's capacity to attach to the surface of the catalyst. For better OER, a considerable overpotential is needed since M-OOH intermediate conversion has sluggish kinetics. Moreover, Adsorption-desorption at active sites of TM-LDH i.e., transition metal components [M], resulting in producing [M–OH], [M–O], and [M–OOH] intermediates start and proceeds the mechanism of the reaction [44, 65, 66].

Sahoo et al. reported that electrocatalytic OER has a mixed and complicated electrocatalytic process involving H^+ and $4e^-$ in both alkaline and acidic environments. However, to demonstrate high OER efficiency, In each stage, there is a respective barrier for Gibbs free energy (ΔGn, where n = 1, 2, 3, and 4) that needs to be overcome, as illustrated in **Fig. 1.7**.

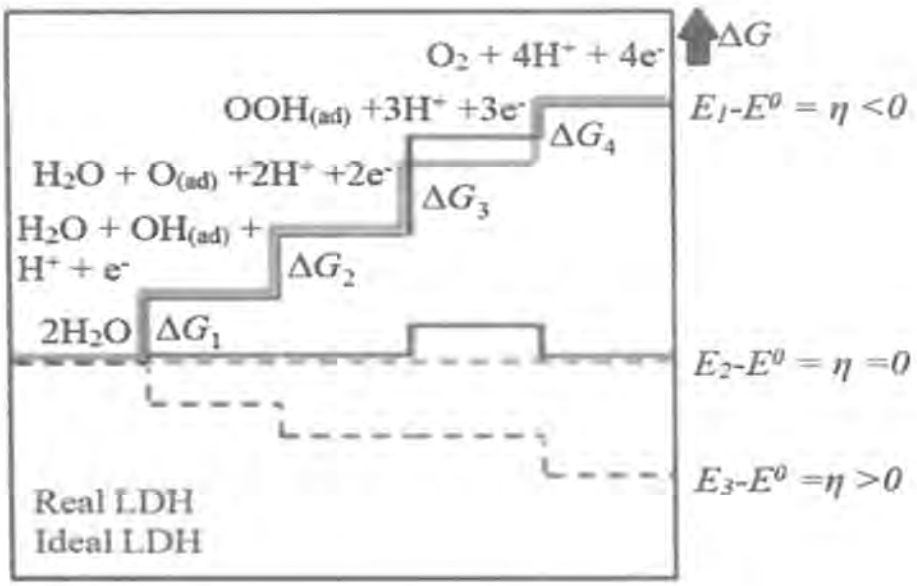

Fig. 1.7 Reaction coordinates vs. Gibbs free energy, comparison for ideal and real TM-LDH for OER[44].

OER process involving TM-LDH is graphically depicted by plotting Gibbs free energy against reaction coordinates. The ΔG_3 shows, a thermochemically unfavorable stage for the real OER catalysts when the M-OOH species are haphazardly connected to the catalyst [3, 44].

1.8 Application of TM-LDH

The ability to alter metal compositions, regulate the molar ratio of M^{3+} and M^{2+} in brucite layers, alteration in layered structure, go through geometric transformations, have a special 2D lamellar structure, exchange intercalated anions, make various host-guest assemblies using nano-design principles, and exfoliate TM-LDHs into 2D nanosheets are all capabilities that help in the development of desirable physicochemical properties [3]. TM-LDH has received considerable attraction in the research field because of many advantages such as abundant precursor sources, high catalytic activity for OER, stability, affordability, and a facile synthesis process.

Moreover, with their flexible, modifiable chemical composition and adaptable structure, these TM-LDH nanomaterials have numerous potential uses [67]. Some of these are enumerated as follows:

- Beyond their use in OER, there are several other electrocatalytic uses of 2D TM-LDHs that are worthwhile to investigate. These applications have substantial relevance in both academic research and industry contexts. These include HER for producing hydrogen, the carbon dioxide reduction reaction (CO_2RR) for producing carbon monoxide (CO) as an environmentally friendly fuel, Oxygen Reduction Reaction (ORR) for producing H_2O_2, the Nitrogen Reduction (NRR) for producing ammonia (NH_3), and the selective oxidation of organic compounds to synthesize value-added products [67].
- LDH-based systems have widespread applications in areas such as drug delivery adsorption, artificial photocatalysis, metal-air batteries, and supercapacitors [68-72].
- LDH materials have emerged as the preferred choice for semiconductor photocatalysis due to their numerous advantages, such as a stable chemical composition, substantial specific surface area, non-toxicity, ease of synthesis, a narrow energy band gap, and a well-structured layered composition, and strong charge separation abilities [73, 74].

- These ionic clays are also used in many of other industries and fields, like in biotechnology, energy storage, fuel cells, medicine (particularly in drug delivery and release), and environment remediation (to clean up pollution) [75].
- LDHs are currently attracting more attention because of their capabilities for anticancer applications, superhydrophobic surfaces, carbon capture, biosensors and adsorbents for water purification and treatment, resistance corrosion electrodes, ion exchangers and adsorbents, in thin film and for water treatment and purification [76-78].

1.8.1 Limitations of TM-LDHs

Some problems limit the electrocatalytic performance of TM-LDHs such as low density of active sites, decreased intrinsic activity, poor conductivity, bulk thickness, and slow ion transport rate. Electrocatalyst activity in water-splitting process is often influenced by number of active sites and intrinsic activity [3]. These factors suppress the high intrinsic activity of these catalysts. So, there are two successful methods to increase electrocatalytic activity:

- Incorporating additional active sites per gram into the catalyst structure or improving catalyst loading to increase the number of active sites on a certain electrode.
- Increasing each active site's natural capacity for catalysis [79, 80].

More specifically, combining these two methods singly can increase catalyst activity through synergistic effects and lead to a considerable improvement in electrocatalysis.

1.9 Various methods to enhance the electrocatalytic efficiency of TM-LDH

Scientists have employed a range of approaches to tackle the challenges arising from the limited electrical conductivity of LDHs. Surprisingly, many LDH-based Catalysts can be synthesized through diverse methods such as, exfoliating dense materials to create thin nanosheets, construction of porous structures, vacancy with defect induction, anion exchange, and changing the distance between layers, using non-metals for doping, modification of surface, hybrid architecture utilizing metal complexes, regulating their morphology and their hybridization with conductive supports. All of these approaches contribute significantly and synergistically to the production of efficient LDH-based OER electrocatalysts [3, 44, 65].

1.9.1 Heterostructure carbon-based materials and TM-LDH

Building LDH and other materials into a heterostructure, which is based on the distinct qualities of several materials, allows for the use of both their advantages as well as the synergistic effects of their combination. Carbon nanotube (CNT) and graphene materials often have excellent electrical conductivities. Therefore, the weak conductivity of LDH can be compensated for by including it in a composite framework. Furthermore, the improved OER activity can be linked with the electron transport between carbon materials and LDH. Various heterogeneous composite structures made of LDH and carbon materials have now been successfully synthesized and work exceptionally well. Generally speaking, nanocarbons offer a substantial surface area and electrically conductive paths to the loaded LDHs. Additionally, it can manage the clustering of LDH crystals [65, 81, 82].

1.10 Graphene oxide (GO)

GO is a two-dimensional substance where the sp^2-C basal plane incorporates O functional groups, distinguishing it from graphene as an oxidized variant. Unlike graphene, which is inherently hydrophobic, GO is hydrophilic, allowing it to disperse easily in aqueous solutions due to the presence of these O functional groups. GO is a desired substance that is employed in a variety of industries is employed in the production of composite materials, renewable energy devices, and electronics (sensors and transparent conductive films) and has uses in biology, and medicine due to tuning of its size from a few nm to mm and chemical characteristics [83].

1.11 Reduced graphene oxide (rGO)

rGO is a nanostructured material that is based on cardon and easily soluble in solutions. It displays notable distinctions from graphene in various aspects, encompassing optical and electronic characteristics, along with its chemical composition. rGO maintains oxygen-related functional groups like hydroxyl carbonyl and epoxy. When rGO is incorporated into inorganic structures to create nanocomposites, it enhances electron transport properties because of rGO's remarkable ability to accept electrons [84].

1.12 Synergistic effect of TM-LDH with rGO

In this regard, Long et al. were the first to discover the coupling of exfoliated FeNi -LDH and graphene oxide (GO) at the molecular level through the utilization of electrostatic attraction, a composite of FeNi-LDH and rGO was successfully synthesized via subsequent reduction, forming FeNi-LDH/rGO. The strong interactions between FeNi-LDH and the integrated rGO effectively and precisely interspersed the LDH layers in an alternating manner. This separation facilitated the exposure of active sites for catalysis and enhanced the flow of charge across the rGO layers, leading to the superior performance for OER [85]. In the context of the TM-LDH/rGO composite, the LDH material is evenly distributed onto the extensive surface area and highly conductive rGO layers. In the realm of electrolysis, this composite demonstrates superior performance in OER when compared to the unmodified TM-LDH and the reference material, IrO_2. Integrating TM-LDH material onto rGO layers offers the potential for two key benefits:

1. The substantial surface area of rGO has the potential to amplify the area of interaction between the LDH and electrolyte, leading to an increase in the active sites.
2. rGO can establish channels for electrical conduction in the NiFe, ultimately boosting the activity of each active site [82].

1.13 Different routes for the synthesis of TM-LDH electrocatalyst

The following is a brief description of some methods that are being utilized for the synthesis of TM-LDH.

1.13.1 Co-precipitation synthesis

The co-precipitation method stands out as the most widely employed technique for fabricating LDH materials, since it just requires one step, has a high yield, and uses inexpensive starting materials. Salt solutions of the bivalent, trivalent, and intercalating anion are combined, stirring continuously. The pH of mixture is kept in optimal alkaline range (pH range 6–11) by mixing in a soda solution, which encourages the concurrent precipitation of cation hydroxide. With the proper pH value and cations ratio, impurity phase development may be prevented. The produced nanohybrids' crystallinity can be improved by a further phase of processing at a moderate temperature (60-80 °C) for a few hours[39, 81]. The mechanism of co-precipitation depends upon the coordination activity

of hexa-aqua metal complexes within the mixed suspension, which is the consequence of the formation of positive sheet resembling brucite like structure, made up of trivalent and divalent cations and interlayer anions with water. A variety of TM-LDHs with their heterostructure and composites have been synthesized for electrocatalytic activity by using the co-precipitation method [3, 87].

1.13.2 Hydrothermal/solvothermal method

The hydrothermal approach is recognized for its operational simplicity and the uncomplicated chemical reactions it entails, which contribute to its success. During this preparation process, the metal salts from the precipitator are mixed with the solvent inside a Teflon container, and the resultant solution is subsequently heated to a specific temperature. Typically, solvents (like water, N-methyl pyrrolidone, dimethyl formamide dimethyl sulfoxide, , ethanol, and methanol) are used to mix precipitating agents like ammonia[88], hexamethylenetetramine (HMT)[89], methanol[90], urea[91] ,$NaOH/Na_2CO_3$ [92] etc., and some structure-directing substances like acetyl trimethyl and NH_4F, under heating.

The precipitator plays a crucial role in this process by providing the essential hydroxyl anions necessary for attracting metal ions and initiating the formation of metal hydroxides, which marks the initial stage of nucleation. Additionally, it aids in the development of layered structures in the subsequent hydrothermal treatment. Altering the reaction conditions, such as pressure, temperature, and reaction duration, LDH nanocrystal morphology, size, and structure can be smoothly controlled in this method. Moreover, a second hydrothermal treatment can be used to synthesize self-supported LDHs or doping and heterostructure-constructed LDHs [3]. This method is widely used because it's feasible and cost-effective.

1.13.3 Electrodeposition

The electrochemical deposition process is an effective way to produce nanostructure electrocatalysts. This procedure is commonly utilized for the production of self-supported LDH films on conductive substrates, this method employs either a two or three-electrode setup. Within this approach, the conductive surfaces serve as the cathodic working electrode during the electro-precipitation process. Concurrently, a metal-

containing aqueous solution is introduced, typically containing metal ions derived from nitrate or sulfate solutions, is utilized as the electrolyte [3]. By employing a negative potential, a cathodic current is achieved due to water reduction, as expressed in the **equation 1.7** :

$$2H_2O + 2e^- \rightarrow H_2 + 2OH^- \quad (1.7)$$

The deposition process is achieved by converting nitrate/sulfate ions into hydroxide ions, resulting in an increase in the pH level in the immediate vicinity of the working electrode... This causes the formation and precipitation of LDHs with similar properties. The characteristics of the LDHs, like their configuration, shape, phase, degree of crystallinity, and thickness on the conductive base, can be precisely adjusted by managing a range of factors. These factors include the applied voltage, current strength, temperature, duration of operation, pH levels, and the concentration of the metal salt solution [93, 94].

1.14 Literature survey

TM-LDHs have been the subject of thorough investigation within the realm of electrocatalysis, particularly for their prospective application as catalysts in OER. Extensive research efforts have been focused on investigating the functions and contributions of TM-LDH as an OER electrocatalyst from the mid-2000 and many aspects in this regard are still unknown, so this is a rapidly growing field of research.

(Jiang et al., 2015) reported NiCo-LDH nanosheets produced by directly growing them on substrate made of nickel foam. These nanosheets exhibit better performance in the (OER) within an alkaline environment. This electrocatalyst featured a remarkably good OER activity a mere 290 mV low onset overpotential, an overpotential of 420 mV is achieved a current density of 10 mA cm^{-2}, which is close to the overpotential needed for the RuO_2 catalyst. Additionally, it demonstrates long-term durability and maintains a significant anodic current density in a 0.1 M KOH solution. The exceptional OER performance of these NiCo-LDH nanosheets can be ascribed to their distinctive redox characteristics and intrinsic layered structure[64].

(Xiaowen et al., 2015) employed electrodeposition technique to produce nanoplates of Ni-Fe LDH on electrochemically rGO in three dimensions for water

oxidation. The electrode displayed a minimal overpotential of 259 mV at a current density of 10 mA cm^{-2}, along with low Tafel slope of 39 mV dec^{-1}. These characteristics render it a suitable candidate for serving as a primary catalyst for OER in an alkaline environment, making it suitable for use as a direct catalyst for OER in an alkaline medium without the using a conductive additive or binder. It is more effective than the costly IrO_2 catalyst concerning its electrochemical durability, reaction kinetics, and effectiveness [95].

(Han et al., 2016) coupled CoFe-LDH with rGO, resulting in a 2D integrated structure known as CoFe-LDH/rGO nanocomposite. The configuration substantially reduces the overpotential needed to achieve a current density of 10 mA cm^{-2} in OER, lowering it to 325 mV in 0.1 M KOH. Moreover, due to their enhanced abilities in transporting mass and charge, coupled with their high structural stability, these nanohybrids showed remarkable durability. The incorporation of these alternating components gives CoFe-LDH/rGO nanocomposite the potential to function as cost-effective highly efficient catalysts, easily available earth-abundant materials for a variety of water-related application [96].

(Feng et al., 2017) Co-based LDH materials incorporating both Fe and Al were synthesized using efficient coprecipitation method. In these catalysts, the presence of trivalent species, Fe^{3+} and Al^{3+}, plays a crucial role in stabilizing the LDH structure, as confirmed through comprehensive characterization employing various surface and bulk-sensitive techniques. Their performance in OER was assessed using rotating disk electrodes. Notably, for Co-Al-based LDH catalysts, an increase in Al content correlated with a decrease in OER activity. Conversely, in the case of Co and Fe-based LDH (CoFe-LDH), a synergistic effect was observed, particularly with an optimal Fe content of 35%. This specific catalyst was applied through a spray-coating process onto Ni foam electrodes, exhibiting exceptional stability within a flow-through cell. It achieved an approximate overpotential of 350 mV@10 mA cm^{-2} and featured a Tafel slope of 49 mV dec^{-1} in a 0.1 M KOH solution [97].

(Wang et al., 2017) fabricated an electrocatalyst by depositing NiFe-LDH nanoparticle (3-5 nm) onto Co, N-codoped carbon nano frames (Co, N-CNF). This electrocatalyst, known as NiFe-LDH/Co, N-CNF, exhibited a Tafel slope of 60 mV dec^{-1}

and an overpotential of 312 mV at 10 mA cm^{-2}. This performance resulted from the combined OER activity of NiFe-LDH and the enhanced conductivity provided by Co, N-CNF [98].

(Liu et al., 2017) designed ultrathin nanosheet arrays of NiCo-LDH on a three-dimensional (3D) porous structure using hydrothermal technique. These nanosheets functioned as a bifunctional catalyst for overall water electrolysis, representing a pioneering application. The distinctive hierarchical 3D porous design, consisting of 2D ultrathin nanostructures, provided several benefits, including enhanced diffusion of active species, increased number of active sites and better charge transport. Consequently, the NiCo-LDH/NF catalyst exhibited outstanding catalytic efficiency and durability in both HER and OER.

In a 1.0 M KOH solution, it achieved a low overpotential of 162 mV for HER and 271 mV for OER, enabling a current density of 10 mA cm^{-2}. Furthermore, the NiCo-LDH/NF catalyst achieved a current density of 10 mA cm^{-2} at a remarkably low cell voltage of 1.66 V, matching the performance of previously reported catalysts for bifunctional water splitting. This research opens up new possibilities for leveraging transition metals to advance the field of overall water splitting [99].

(Feng et al., 2017) synthesized active CoFe-LDH and observed its OER activity in 1M KOH. This catalyst on nickel foam substrate (CoFe-LDH) exhibited η of 300 mv@10 mA cm^{-2} and on ITO (indium tin oxide) substrate the η was 400 mV and estimated Tafel slop of 83 mV dec^{-1} [57].

(Yang et al., 2020) performed hydrothermal synthesis of nanocomposite called CoFe-LDH/MWCNT/rGO, which proves to be active bifunctional electrocatalyst, supporting both OER and the Oxygen Reduction Reaction (ORR). The inclusion of MWCNT and rGO alongside CoFe-LDH in this nanocomposite introduces a hierarchical porous structure and boosts conductivity, greatly aiding efficient mass transport and charge transfer during OER and ORR processes.

In practical terms, CoFe-LDH/MWCNT/rGO displayed impressive OER performance in a 1 M KOH solution, with a low onset overpotential of 330 mV. Moreover,

it required an overpotential of 430 mV to achieve a current density of 10 mA cm^{-2}. Additionally, this nanocomposite exhibited excellent catalytic activity for ORR, with an onset potential of 708 mV vs. RHE in a 0.1 M KOH solution and a preference for the 4-electron pathway. The exceptional bifunctional catalytic performance of CoFe-LDH/MWCNT/rGO in both OER and ORR results from the synergistic effects stemming from the incorporation of MWCNT, rGO, and CoFe-LDH [100].

(H. Sung et al., 2020) synthesized NiCo-LDH nanowires and investigated their performance in (OER. The electrochemical assessments were conducted in a 1 M KOH solution, revealing an overpotential of 250 mV @10 mA cm^{-2} and a Tafel slope of 89 mV dec^{-1} [62].

(Wang et al., 2021) Reported an OER electrocatalyst of NiFe-LDH nanosheets with oxygen and metal multivacancy showed η = 230 mV at 100 mA cm^{-2}. a Tafel slope of 37.1 mV dec^{-1} [101].

(Yunqi et al., 2021) fabricated NiFe-LDH and analyzed its OER activity in 1 M KOH and calculated η = 342 mV at 10 mA cm^{-2} and Tafel slope of 57.4 mV dec^{-1} [102].

(Guo et al., 2021) A composite material comprising CoFe-LDH nanosheet arrays grown on rGO-modified Ni foam was successfully produced using a citric acid-assisted aqueous phase co-precipitation technique. Comprehensive analysis revealed that all compositions within the CoxFe1-LDH/rGO/NF series (where x = 4, 3, 2) featured CoxFe1-LDH nanosheets growing vertically on the surface of the rGO-modified Ni foam. Significantly, among this series, the Co_3Fe_1-LDH/rGO/NF composite demonstrated the most impressive performance. It exhibited overpotentials of 250 mV for OER and 110 mV for HER at a current density of 10 mA cm^{-2} in a 1 M KOH solution. When serving as both the cathode and anode concurrently in the process of complete water splitting, it requires cell voltages of 1.65 V and 1.84 V at current densities of 10 mA cm^{-2} and 100 mA cm^{-2}, respectively. The remarkable performance of Co_3Fe_1-LDH/rGO/NF can be ascribed to its nanosheet array architecture. Several pivotal factors contribute to its exceptional catalytic efficiency:

1. The distinctive nanosheet array structure featuring open channels, which provides an abundance of accessible active sites.

2. The synergistic cooperation between Co_3Fe_1-LDH and rGO, enhancing electrochemical performance and elevating electrical conductivity.

3. The in-situ growth of Co_3Fe_1-LDH on rGO/NF aids in the release of gas bubbles and greatly enhances long-term stability [103].

(Wan et al., 2022) fabricated NiFe LDH@SnO_2/NF composite, this electrocatalyst demonstrated efficient OER activity, obtaining a low η of 234 mV@10 mA cm^{-2}. Long-term stability testing revealed no voltage fluctuations over a 12-hour operation @100 mA cm^{-2}, confirming its stability [104].

(Wang et al., 2023) designed a method of fabrication of CoP@NiCo -LDH samples through a multi-step growth method, and CoP@NiCo LDH-100 displayed remarkable electrocatalytic performance. Specifically, it achieved a minimal overpotential of 68.7 mV for HER and an overpotential of 225 mV at 50 mA cm^{-2} for OER in 1 M KOH electrolyte, with outstanding stability over 50 hours [105] .

According to the literature review, it is obvious that to date, numerous TM-LDHs OER electrocatalysts have been fabricated using diverse synthetic techniques. This points to two crucial aspects: (a)TM-LDH electrocatalysts have promising potential as OER electrocatalysts and (b) there is still room to get its optimized form to commercialize it as an electrocatalyst. This prompted us to design the current study, with the hope that the results of this work may aid in further understanding of the potential material.

1.15 Aims & plan of research work

The primary objective of this project was to synthesize an OER active material that is eco-friendly, cost-effective, earth-abundant, and can show significant stability in an alkaline medium. For this purpose, TM-LDH materials (CoFe-LDH, NiCo-LDH and NiFe-LDH) and their composites with rGO (CoFe-LDH/ rGO, NiCo-LDH/ rGO, NiFe-LDH/ rGO) were selected and following objectives were taken into consideration.

- To synthesize NiFe-LDH, NiCo-LDH, and CoFe-LDH materials via a simple and cost-effective hydrothermal route.
- To modify the above synthesized LDH materials by reduced graphene oxide to obtain, NiFe-LDH/rGO, CoFe-LDH/rGO, and NiFe-LDH/rGO composites via the same hydrothermal route.
- To determine the electrocatalytic efficiency of these synthesized catalysts for OER through studying various kinetic parameters such as overpotential, Tafel slope, etc.

In the work plan the first step was synthesis of TM-LDHs composites with (CoFe-LDH, NiCo-LDH and NiFe-LDH) and their composites with rGO (CoFe-LDH/rGO, NiCo-LDH/rGO, NiFe-LDH/rGO) by cost effective and simple hydrothermal method.

In the second step, catalyst ink was prepared for each electrocatalyst and applied on a glassy carbon (GC) electrode. Which was subjected to electrochemical investigations. Next these modified GC electrodes were then analyzed through LSV, CV, and EIS to investigate the OER activity of all the synthesized electrocatalysts. The data were obtained, and the critical parameters were calculated to evaluate the activity of the synthesized nanomaterials. The obtained results were interpreted and compared with the reported work.

Chapter 2

EXPERIMENTAL

The present work aims to synthesize layered double hydroxides based on transition metals (CoFe-LDH, NiCo-LDH and NiFe-LDH) and their composites with reduced graphene oxide(CoFe-LDH/rGO, NiCo-LDH/rGO, NiFe-LDH/rGO) as OER electrocatalysts to be used in alkaline water electrolyzer for hydrogen evolution. This chapter covers information regarding all experimental work performed during this research work. It includes information about the utilized chemicals and reagents, details of different adopted synthetic procedures and employed instrumentations and techniques, systematically.

2.1 Chemicals and reagents

The reagents and chemicals used in this research work are mentioned in **Table 2.1**, along with their specifications and source.

Table 2.1: List of chemicals and reagents with their specifications.

Sr No.	Chemicals/Reagents	Molar mass (g/mol)	Mass purity (%)	Source
1.	Nickel(II) nitrate hexahydrate	290.79	99	Sigma- Aldrich
2.	Nickel(II) acetate tetrahydrate	248.84	99	Sigma- Aldrich
3.	Cobalt(II) nitrate hexahydrate	291.03	98	Sigma- Aldrich
4.	Cobalt(II) acetate tetrahydrate	249.08	99	Merck
5.	Hexamethylenetetramine	140.19	98	Sigma- Aldrich
6.	N, N-Dimethylformamide	73.09	99	Sigma- Aldrich
7.	Urea	60	99	Fluka
8.	Iron(III) nitrate nanohydrate	404	99	Sigma- Aldrich

9.	Potassium hydroxide	56.10	99	Sigma- Aldrich
10.	Graphite flakes	12.011	99.9	Sigma- Aldrich
11.	Potassium permanganate	158.03	99	Merck
12.	Hydrogen per oxide	34.01	30	Sigma- Aldrich
13.	Sodium nitrate	84.99	99	Sigma- Aldrich
14.	Hydrochloric acid	36.45	37	Merck
15.	Sulphuric acid	98.09	95-97	Sigma- Aldrich
16.	Hydrazine	32.04	65	Merck
17.	Ethanol	46	99.1	Analar
18.	Isopropanol	60	99.7	Analar
19.	De-ionized water	18	-	-

2.2 Instrumentation

This section includes the details of all instruments and techniques namely X-ray diffraction (XRD), fourier-transform infrared spectroscopy (FTIR), centrifugation, sonication, and magnetic stirring, and describes the setup of the electrochemical workstation, utilized for the synthesis and characterization of desired electrocatalysts.

2.2.1 X-ray diffraction (XRD)

The crystallographic and structural evaluation of synthesized material can be done by XRD. It has the potential to be an effective technique for identifying crystalline or semi-crystalline compounds. The established X-ray diffractograms produced from comparable JCPDS (Joint committee on powder diffraction standards) references available in the ICDD (International center for diffraction data) repository are compared to the X-ray diffraction patterns of synthesized materials. Along with its ability to identify materials, XRD examination also reveals information about phase, crystal alignment, structure, and characteristics related to structure, such as average crystallite size, flaws, and stress [106].

For structural analysis of synthesized transition metal-based LDH (TM-LDH) material, their composite with rGO and graphene oxide (GO), an X-Ray diffractometer (Spectris Company Australia) model PANalytical 30440/60 X pert PRO was employed. By applying the voltage at 40 KeV and current at 40 m A, the Cu-Kα X-ray source was used for evaluation at a scan rate of 0.01° /sec over 2θ values ranging from 10°-80°. A finely powdered form of synthesized LDH material was subjected to XRD analysis. The Debye-Scherrer equation has been used to determine the average crystalline size, as shown in **equation 2.1** :

$$D = \frac{k\lambda}{\beta cos\theta} \qquad (2.1)$$

k is Scherrer' s constant taken about 0.9, D represents the size of the crystallite (nm), λ denotes the wavelength of X-ray, and in the case of copper's Kα its value is 0.154 nm , β signifies the full width at half maximum (FWHM) of the diffraction peak (in radian) and θ denotes the Bragg's diffraction angle.

2.2.2 Fourier -transform infrared spectroscopy (FTIR)

FTIR is an important technique in identifying the functional groups present in each sample. Functional groups and vibrational modes of all synthesized TM-LDH material were investigated using FTIR in frequency ranging 400-4000 cm^{-1} using provided by Thermo Scientific (NICOLET 6700). All the synthesized materials were analyzed by employing a resolution rate of 0.4 cm^{-1}.

2.2.3 Centrifuge and sonicator

Extensive washing and separation of all synthesized materials was carried out by Hermle Labortechnik Z 206A centrifuge at 200-6000 rpm.

The Elma Sonic E30H sonicator with a frequency of about 50/60 Hz and power of 240 W was used to get a homogenous mixture of products for further proceedings.

2.2.4 Electrochemical workstation

All the electrochemical techniques i.e., electrochemical impedance spectroscopy, cyclic voltammetry and linear sweep voltammetry were carried out on a Gamry Interface 1000E (Louis Drive Warminster, PA 18974, USA) equipped with Gamry Framework 6.03 software. This Gamry potentiostat model 1000E is a high-performance electrochemical workstation that can operate well in both the potential control range (±1 mV, ±0.2% of setting and reading) and the current control range (±5 pA, ± 0.3% of range).

Fig. 2.1 A photograph of electrochemical cell setup.

The voltametric cell used for this research work was a 50 mL glass vial with a Teflon cap having three standard taper ports for inserting the electrodes within the cell as depicted in **Fig. 2.1**. All electrochemical analyses were carried out using an electrode system and 1 M aqueous KOH was used as an electrolyte. The electrodes used are described below:

1. Working electrode: Modified glassy carbon (GC) electrode with an area of 0.0707 cm^2.

2. Counter electrode: Pt wire having a length of 37 mm and diameter of 0.5 mm.

3. Reference electrode: Saturated calomel (Hg/Hg_2Cl_2/ KCl).

The reaction under consideration takes place on working electrode. As in present work, OER is under examination so modified glassy carbon functions as an anode. The circuit is completed by counter electrode. At the counter electrode, reaction opposite to that on the working electrode takes place here. To reduce the ohmic drop or IR drop effect, a minimal distance was maintained between the working and reference electrodes [107].

2.3 Experimental procedure

This section covers the methods followed for synthesis of graphene oxide, TM-LDH materials including CoFe-LDH, NiCo-LDH and NiFe-LDH, their composite with reduced graphene oxide (CoFe-LDH/rGO, NiCo-LDH/rGO, NiFe-LDH/rGO) and fabrication of working glassy carbon electrode.

2.3.1 Synthesis of graphene oxide

The synthesis of graphene oxide was completed by employing modified Hummer's method, as shown in **Fig. 2.2** [108].

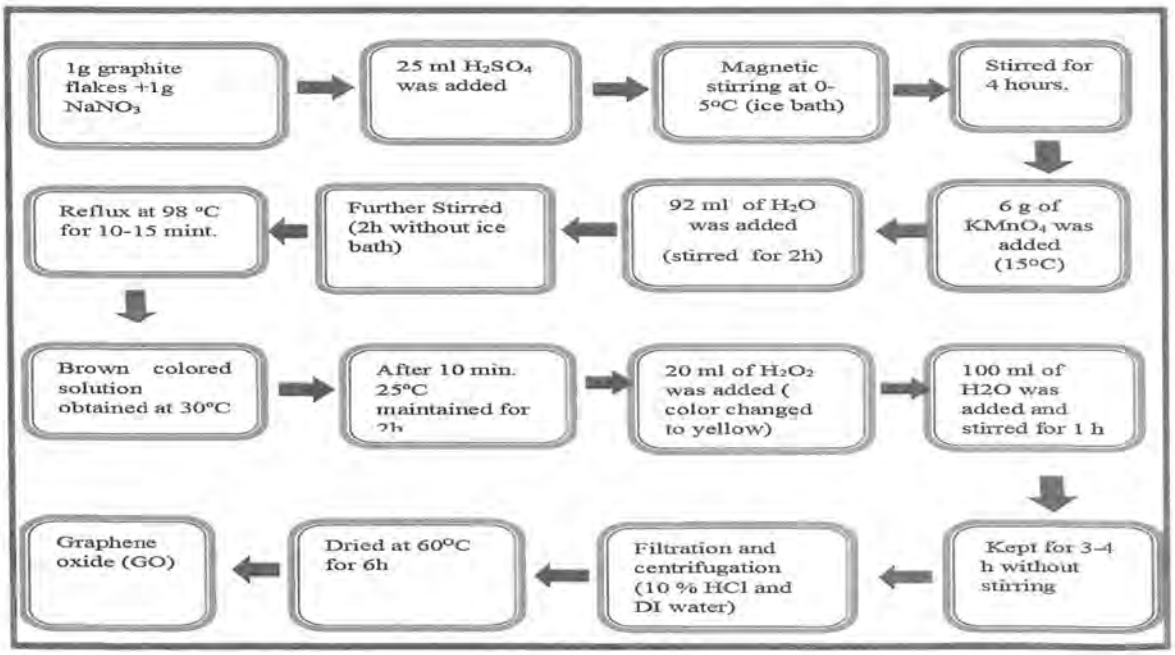

Fig. 2.2 Schematic diagram representing the synthesis of GO by modified Hummer's method.

2.3.2 Synthesis of TM-LDH materials (CoFe-LDH, NiCo-LDH and NiFe-LDH)

The synthesis of TM-LDH electrocatalysts (CoFe-LDH, NiCo-LDH, NiFe-LDH) were carried out by utilizing hydrothermal method [104, 105]. To synthesize NiFe-LDH, a homogenous mixture containing 0.02 M of $Ni(NO_3)_2 \cdot 6\ H_2O$ and 0.01 M of $Fe(NO_3)_3.9H_2O$ in 50 DI water (1:2 of Fe^{3+} and Ni^{2+}) was prepared. After this a solution of hexamethylenetetramine (HMT, 0.5g/20 mL) was added to the above mixture steadily while constant stirring at room temperature. Then this mixture was shifted into a Teflon lined autoclave (100 mL) and placed in preheated oven at 180 °C for time period of 12 hours. After completing the reaction time, autoclave was naturally cooled to ambient temperature. After this, thoroughly washing of obtained product with deionized water and ethanol and then dried at 50 °C overnight to yield NiFe-LDH. The synthesis of CoFe-LDH and NiCo-LDH was performed by the similar above-mentioned procedure simply by altering the precursors. Such as, for the synthesis of CoFe-LDH cobalt nitrate hexahydrate and iron nitrate nano hydrate were used as precursors. In the synthesis of NiCo-LDH cobalt nitrate hexahydrate and nickel nitrate hexahydrate were used as precursors and treated with HMT.

In this synthesis procedure, a one-pot hydrothermal approach was used for producing nitrate-intercalated TM-LDHs utilizing HMT as a hydrolysis agent. The HMT was important in this approach because it supplied hydroxyl anions (HMT acts as a hydrolysis agent and base) that were attached with metal ions for formation of metal hydroxides. This was primary nucleation step helped in the construction of layered structure in subsequent hydrothermal procedure [110].

2.3.3 Hydrolysis of HMT

Equation 2.2 and **2.3** depict the hydrolysis of HMT ($C_6H_{12}N_4$)

$$C_6H_{12}N_4 + 6H_2O \rightarrow 4NH_3 + 6HCHO \qquad (2.2)$$

$$NH_3 + H_2O \rightleftharpoons NH_4^+ + OH^- \qquad (2.3)$$

HMT was intended to hydrolyze in an aqueous solution at high temperatures, releasing ammonia and making the solution alkaline. Ammonia and formaldehyde are produced during the hydrolysis of HMT and are not incorporated into the LDH [106]. HMT

acts as a hydrolysis agent, which means it reacts with water molecules to release hydroxide ions, which take part in generation of structure of LDH. Hydrolysis is a chemical process that involves the cleavage of chemical bonds through the incorporation of water, leading to the formation of new compounds, which is consistent with the process of fabrication of TM-LDH [3].

To summarize this synthesis method, it is concluded that the procedure involved in the breakdown of HMT leads to the release of hydroxide ions. These hydroxide ions then react with metal ions derived from precursor salts, resulting in the formation of layers of metal hydroxides. Subsequently, nitrate ions were introduced into the interlayer space of the LDH structure due to electrostatic interactions. Consequently, TM-LDH was formed, with nitrate serving as anion in its interlayer space.

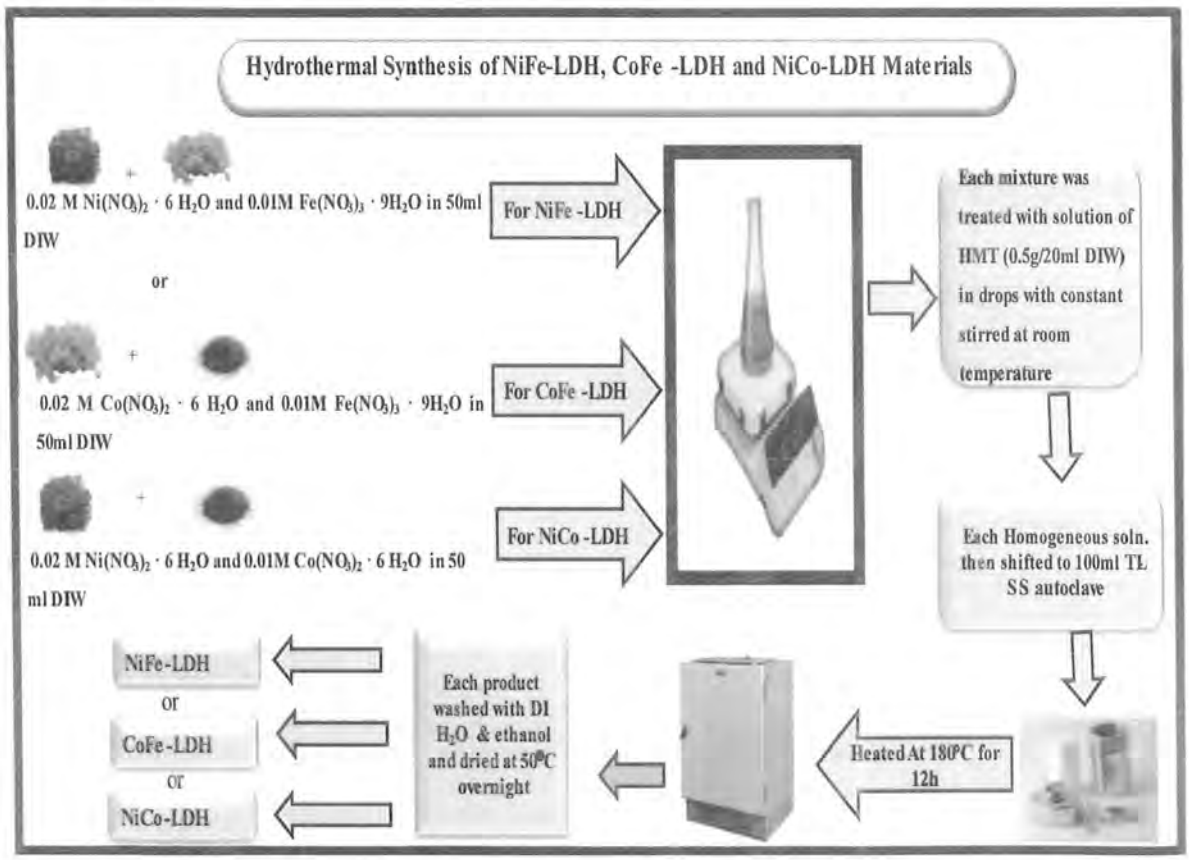

Fig. 2.3 Pictorial representation of synthesis procedure for NiFe-LDH, NiCo-LDH, and CoFe-LDH electrocatalysts by hydrothermal method.

2.3.4 Synthesis of composite of TM-LDHs with rGO (NiCo-LDH/rGO, CoFe-LDH/rGO and NiFe-LDH/rGO)

The synthesis of TM-LDH/rGO composites was done solvothermal process [82, 112]. Initially, GO was synthesized using Hummer's technique then it was dispersed ultrasonically in water(2 mg/mL). To synthesize NiFe-LDH/rGO, the aqueous solutions 0.2 M $Ni(CH_3CO_2)_2.4H_2O$ (20 mL) and 0.2 M $Fe(NO_3)_3.9H_2O$ (4 mL)were mixed, followed by addition of GO solution(12 mL), 24 ml of DI water, 2 M urea solution (5mL DIW) and 30 mL DMF, and 20 uL of 65% hydrazine. Hydrazine was introduced into the solution acting as reducing agent. This entire solution was then shifted to a reactor (stainless -steel autoclave) coated with Teflon and subjected to solvothermal treatment, Initially, at 120 °C for 18 hours, followed by a subsequent step at 160 °C for 2 hours. Following by centrifugation and thorough washing with DI water, the NiFe-LDH/rGO was obtained. The synthesis of NiCo-LDH/rGO and CoFe-LDH/rGo were carried out by the similar above-mentioned procedure simply by altering the precursor salts. For example, in production of CoFe-LDH/rGo the cobalt acetate tetrahydrate and iron nitrate nano hydrate were used as precursors. In the synthesis of NiCo-LDH/rGO the nickel acetate tetrahydrate and cobalt nitrate hexahydrate were used as precursors.

In this synthesis method urea was used as a hydrolysis agent. Normally, urea undergoes hydrolysis when water molecules are present, resulting in the production of carbonate and hydroxyl (OH^-) ions. These ions, in turn, facilitate the formation of metal hydroxide carbonates when metal salts (specifically nitrates) are also present, leading to precipitation. The hydrolysis reaction in the case of urea is as follows:

$$NH_2\text{-}CO\text{-}NH_2 + H_2O \rightarrow 2NH_3 + CO_2 \quad \textbf{(2.4)}$$

$$CO_2 + H_2O \rightarrow CO_3^{2-} + 2H^+ \quad \textbf{(2.5)}$$

$$NH_3 + H_2O \rightarrow OH^- + NH_4^+ \quad \textbf{(2.6)}$$

During hydrothermal reaction, urea undergoes hydrolysis resulting in the formation of NH_3 molecules and CO_2 (**equation 2.4**). These molecules then react with H_2O to give rise to the generation of NH_4^+, CO_3^{2-} and OH^- ions, as shown in **equation 2.5 and 2.6**. Consequently, the OH^- and CO_3^{2-}, species combine with metal salts, leading to a

precipitation phenomenon [112]. Hence TM-LDH/rGO was formed, with CO_3^{2-} serving as the interlayer anion.

It was concluded that HMT serves two functions while undergoing hydrothermal process: (i) as a hydrolysis reagent and (ii) as an inducer, resulting in nitrate ion intercalated into the LDH's interlayer gallery while urea induces carbonate anion in interlayer space of LDH.

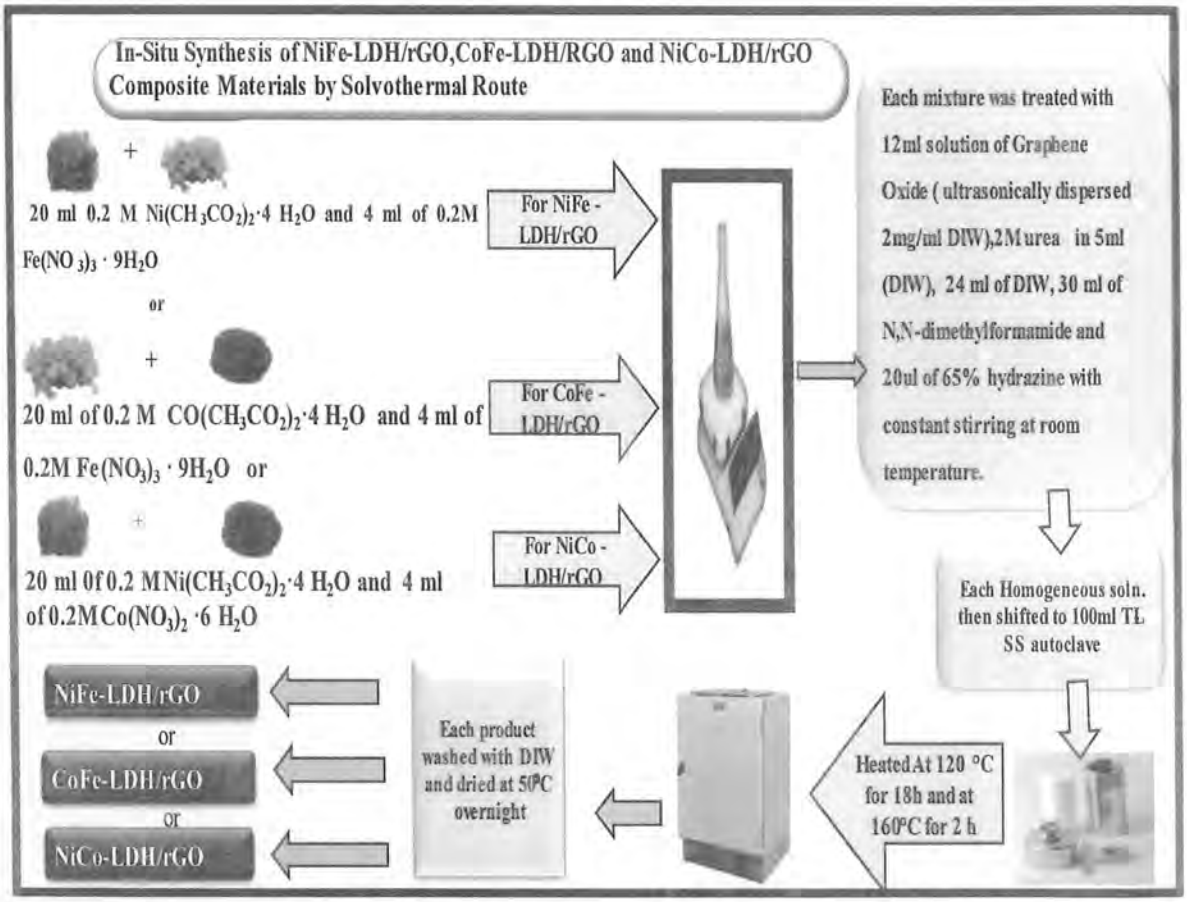

Fig. 2.4 Pictorial representation of synthesis procedure for NiFe-LDH/rGO, CoFe-LDH/rGO, and NiCo-LDH/rGO composites by solvothermal method.

2.3.5 Fabrication process of working electrode

To conduct electrochemical analysis, the synthesized electrocatalysts (NiFe-LDH, NiCo-LDH, CoFe-LDH, NiFe-LDH/rGO, CoFe-LDH/rGO, and NiCo-LDH/rGO were deposited separately on glassy carbon (GC) to fabricate working electrode as depicted in **Fig. 2.5**. For this purpose, 3.5 mg of synthesized powder of catalysts was added to 50 μL

isopropanol. Then 2 µL Nafion was added to this mixture. A slurry was formed through sonication of the above mixture for one hour. Subsequently, using a micropipette, 10 µL of the slurry was deposited on a well-polished GC electrode, and then it was dried completely using a blower. This modified GC electrode was then analyzed through LSV, CV, and EIS to investigate the electrochemical behavior of the synthesized material.

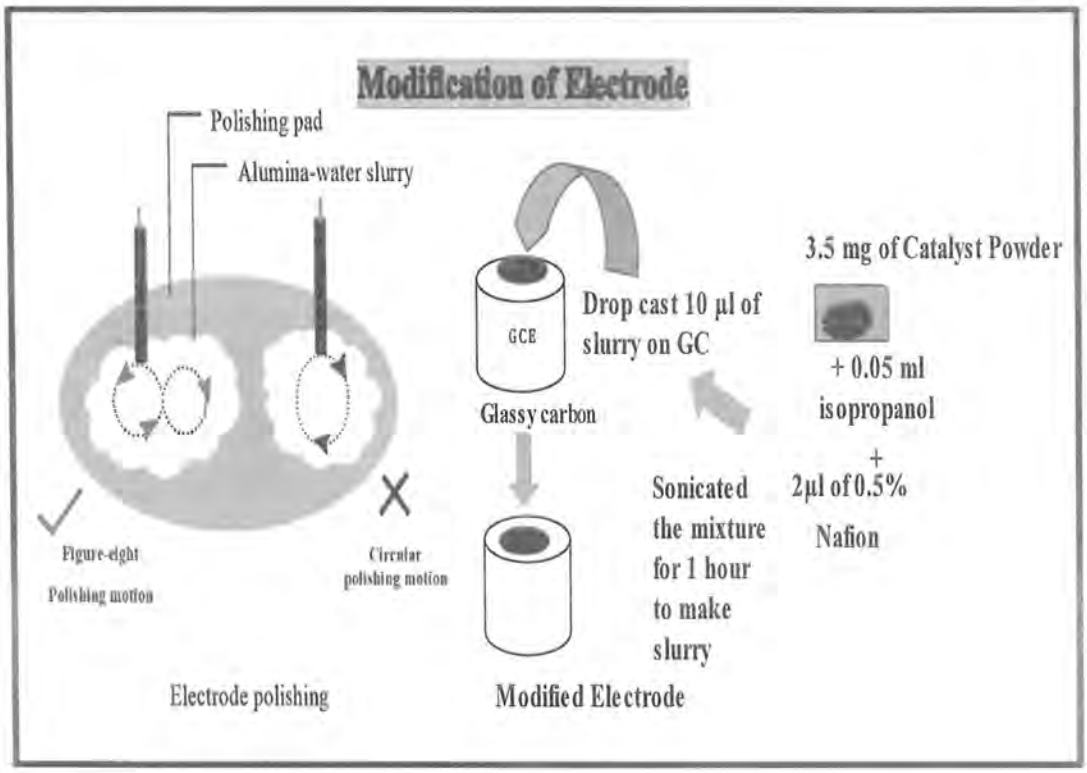

Fig. 2.5 Illustration of the electrode fabrication process.

Chapter 3

Results and Discussion

As previously discussed, the primary goal of this study was to synthesize an effective anode based on TM-LDH for electrochemical water splitting. Six different types of TM-LDHs including three pristine LDHs i.e., CoFe-LDH, NiCo-LDH, and NiFe-LDH and three composites of these LDHs with rGO i.e., CoFe-LDH/rGO, NiCo-LDH/rGO and NiFe-LDH/rGO respectively, were targeted to be synthesized and examined for their electrocatalytic efficiency in the OER. The reported experimental approach (hydrothermal) was used to fabricate the required catalysts. This chapter contains a detailed description of the results acquired from the experimental work performed throughout this research work.

3.1 Structural and crystallographic properties by X-ray diffraction

The synthesized electrocatalysts and GO were subjected to XRD and structural investigation of these materials was conducted through this technique.

3.1.1 XRD analysis of graphene oxide (GO)

The XRD pattern of GO exhibited sharp and prominent diffraction peak at a 2θ value of 11.33° corresponding to crystal plane (001) as shown in **Fig. 3.1**, confirming the successful synthesis of GO.

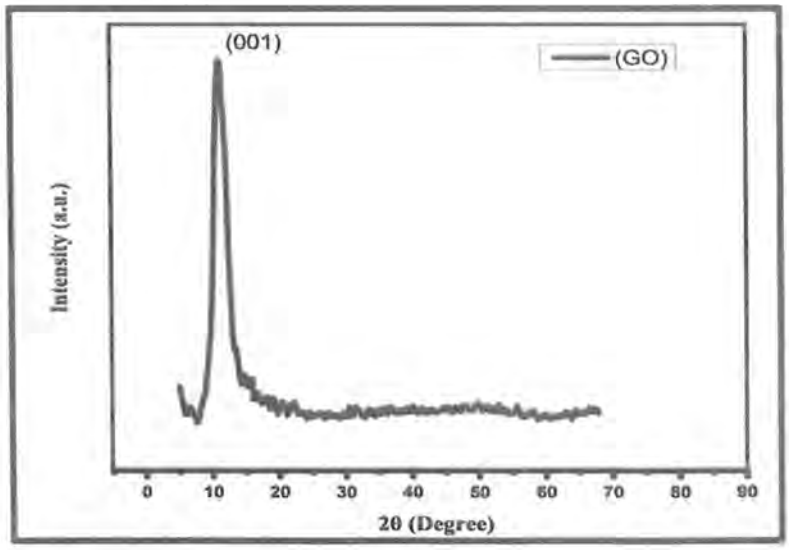

Fig. 3.1 XRD pattern of synthesized GO.

3.1.2 XRD analysis of NiFe-LDH and NiFe-LDH/rGO

The XRD patterns of synthesized NiFe-LDH and NiFe-LDH/rGO composite is shown in **Fig. 3.2**, which corresponds to their reference XRD patterns (JCPDS card No. 40-0215), available in the ICDD database [113]. As no additional phases were found, NiFe-LDH was the dominant phase. The crystalline structure of NiFe-LDH was preserved after combining with rGO as suggested by their similar XRD diffractogram. As rGO displays a characteristic peak at 2θ of 24°, this peak merged with the peak of NiFe-LDH corresponding to (006) hence giving a little broader peak at 2θ value of 23.9° for NiFe-LDH/rGO confirming the presence of rGO and showing successful reduction of GO to rGO.

The peaks positioned at 2θ values 11.2°, 23°, 34.4°,39°, 46.71°, 61° and 62° were indexed as (003), (006), (012), (015), (018), (110) and (113) planes respectively. In case of NiFe-LDH/rGO composite a little peak shift for (003) and (006) planes compared to pristine NiFe-LDH was observed, showing that the d-spacing decreased for these two planes. This decrease in d-spacing was due to the change of interlayer anion as in the case of pristine NiFe-LDH the interlayer anion was nitrate and in the case of the composite the anion was carbonate confirmed by calculating the d-spacing (using the Bragg's equation as shown in **equation 3.1**).

$$n\lambda = 2d \sin\theta \qquad (3.1)$$

where , λ is the wavelength of the incident wave , d is the d-spacing, n is a positive integer and θ is the glancing angle. For the same reflections, the relationship between θ and basal spacing should be:

$$2d_1 \sin\theta_1 = 2d_2 \sin\theta_2 \qquad (3.2)$$

where d_1 and θ_1 are 0.72 , 0.39 nm and 12.34°, 23.9° for the (003) and (006) reflections of NiFe- LDH/rGO (JCPDS Card No. 40–0215) respectively. The tested glancing angles, θ_2 are 11.2° and 23° for pristine LDH. The results of d_2 were calculated as 0.81 nm and 0.4 nm for the (003) and (006) reflections of pristine NiFe-LDH , respectively.

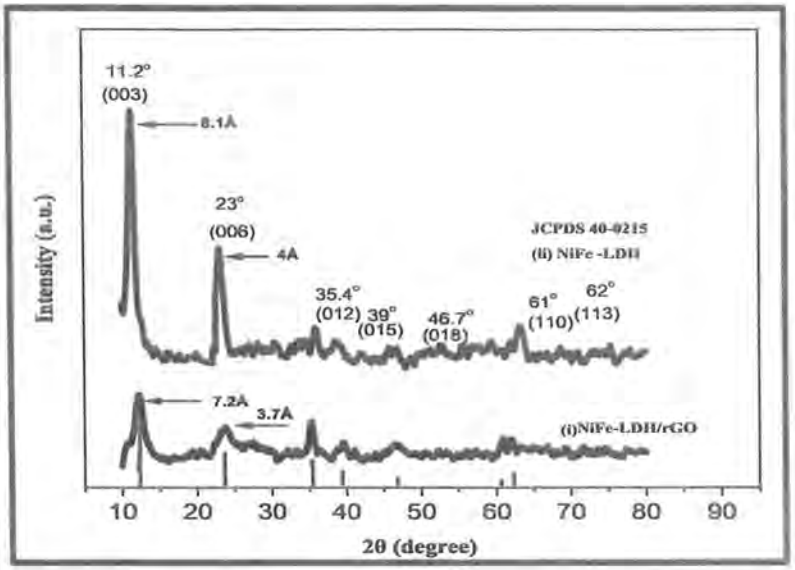

Fig. 3.2 XRD pattern of (i) NiFe-LDH /rGO and (ii) NiFe-LDH.

3.1.3 XRD analysis of CoFe-LDH and CoFe-LDH/rGO

The XRD patterns for CoFe-LDH and CoFe-LDH/rGO composite are shown in **Fig. 3.3**, corresponding to their reference JCPDS card No. 50-0235, available in the ICDD database [114]. As no additional phases were found confirming that CoFe LDH is the dominating phase. The crystal structure of CoFe-LDH was preserved after combining with rGO suggested by their similar XRD diffractogram. The distinct diffraction peaks were appeared at 2θ values of11.05°, 22.4°, 33.9°,35.9°, 45.88°, 60.6° and 61.6° can be indexed as (003), (006), (012), (015), (018), and (110) and (113) crystal planes , respectively. For CoFe-LDH/rGO composite a little peak shift for (003) and (006) planes compared to pristine CoFe-LDH was observed, this showed that the d-spacing decreased for these two planes. This decrease in d-spacing was due to a change of the interlayer anion as in the case of CoFe-LDH, the interlayer anion was nitrate and in the case of CoFe-LDH/rGO, the anion was carbonate (corresponding to the different hydrolysis agent in the synthesis of these materials as discussed earlier in experimental section) as confirmed by calculating the d-spacing by using **equation 3.2**. In this case, d_1 and θ_1 are 0.76 nm, 0.39 nm and 11.39° and 22.42° for the (003) and (006) reflections of CoFe- LDH/rGO (JCPDS Card No. 50–0235) respectively. The tested glancing angles, θ_2 are 11.05° and 22.42° for CoFe-LDH. The results of d_2 were obtained as 0.8 nm and 0.43 nm for the (003) and (006) reflections of CoFe-LDH, respectively.

A broader peak at 2θ value of 22.6° for CoFe-LDH/rGO as compared to CoFe-LDH corresponds to the (006) plane confirming the presence of rGO and shows a successful reduction of GO to rGO.

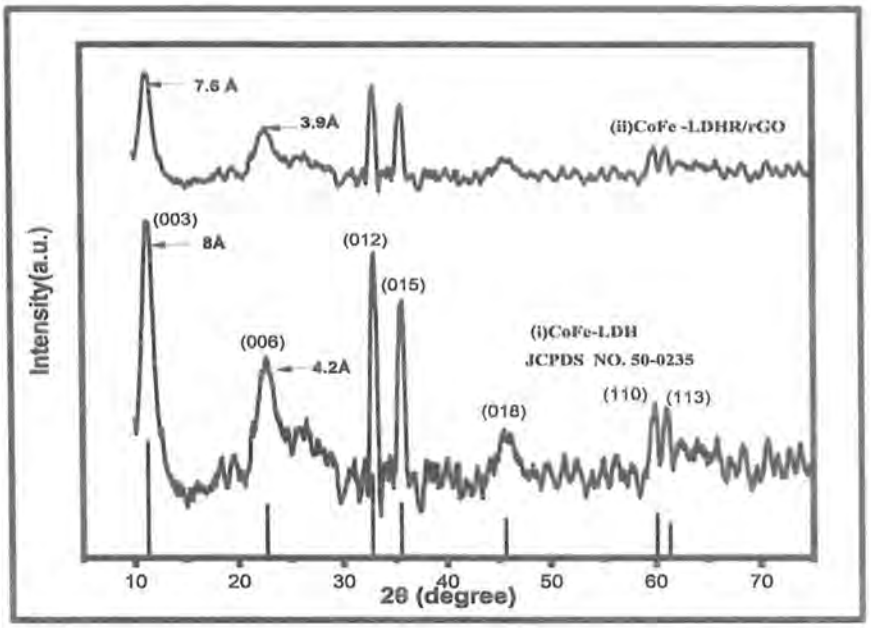

Fig. 3.3 XRD pattern of (i) CoFe-LDH and (ii) CoFe-LDH/rGO.

3.1.4 XRD analysis of NiCo-LDH and NiCo-LDH/rGO

The XRD patterns for NiCo-LDH and Nio-LDH/rGO composite revealed in **Fig. 3.4**, correspond to their reference JCPDS card No. 33-0419 available in the ICDD database [115]. The observed diffraction planes (003), (006), (012), (015), (018), and (110) and (113) confirmed their layered structure. In the case of NiCo-LDH/ rGO composite, a little peak shift for (003) and (006) planes compared to pristine NiCo-LDH was observed, showing that the d-spacing decreased for these two planes because of the change of interlayer anions.

The results of d-spacing for (003) and (006) planes are given as d_1 and θ_1 are 0.77 nm , 0.31 nm and 13.87° and 29.32° respectively for the (003) and (006) reflections of NiCo- LDH/rGO (JCPDS Card No. 33–0419). The tested glancing angles, θ_2 are 13.12° and 26.12° for NiCo-LDH. The results of d_2 were obtained as 0.81 nm and 0.34 nm for the (003) and (006) reflections of CoFe-LDH respectively.

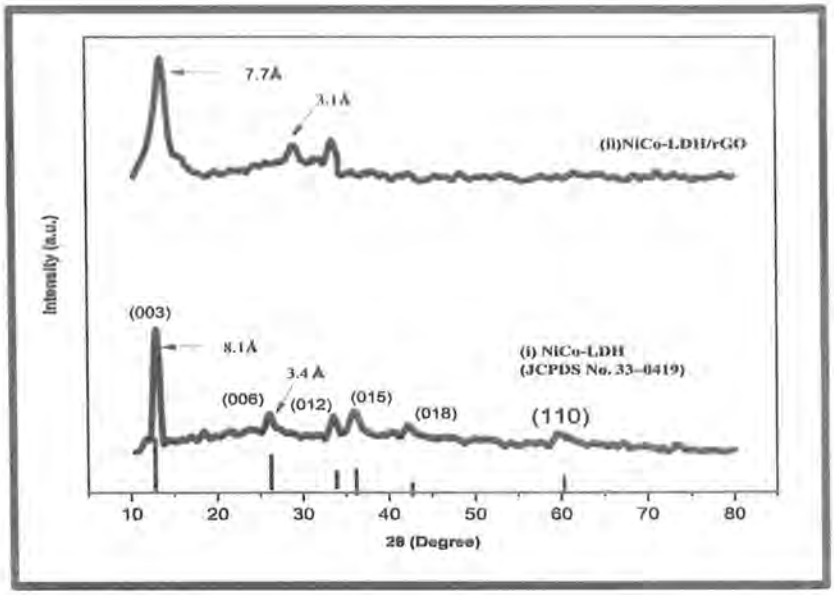

Fig 3.4 XRD pattern of (i) NiCo-LDH and (ii) NiCo-LDH /rGO.

The discussion concludes that all electrocatalysts were successfully synthesized and in the case of pristine TM-LDH, the interlayer anion was nitrate and for their composite with rGO, the interlayer anion was carbonate because of different synthesis conditions as discussed in the synthesis procedure of these materials. While undergoing solvothermal treatment, the crystallization of TM-LDHs and the reduction of GO to rGO occurred simultaneously. Furthermore, crystals of TM-LDHs were preferentially deposited onto the rGO layer, likely because of oxygen containing functional groups. This was confirmed by XRD analysis. All the results relate to the current literature [110].

Furthermore, the average crystalline size of each catalyst was calculated (using the Debye-Scherrer equation, illustrated as **equation 2.1**) as shown in **Table 3.1**, and it was observed that the average crystalline size of composite material was less than the average crystalline size of pristine TM-LDH material. This is probably because of incorporation of rGO during the material synthesis process and different type of interlayer anions for pristine and composite materials. Furthermore, This addition of rGO seemed to enhance the formation of various nucleation sites, leading to a higher density of nucleation for TM-LDHs\rGO. At the same time, it appeared to limit the uninterrupted growth of crystals.

Table 3.1: The average crystalline size of synthesized materials.

S.No.	Sample	The average crystalline size (nm)
1.	NiFe-LDH	14.4
2.	NiFe-LDH/rGO	10.0
3.	COFe-LDH	22.0
4.	CoFe-LDH/rGO	17.4
5.	NiCo-LDH	13.5
6.	NiCo-LDH/rGO	11.0

3.2 Fourier-transform infrared spectroscopy (FTIR) analysis

The structural difference between bare TM-LDHs and their composite was investigated using FTIR spectroscopy. The FTIR spectra of all synthesized materials exhibited peaks indicating the presence of carbonate ions (in composites), nitrate ions (in pristine TM-LDHs), and water molecules in the layered structure of all LDHs.

3.2.1 FTIR analysis of NiFe-LDH and NiFe-LDH/rGO

In the case of Ni-Fe combination of LDH, the FTIR spectra **[Fig. 3.5 (a) and (b)]** depicted the characteristic peaks for NiFe-LDH and NiFe-LDH/rGO composite.

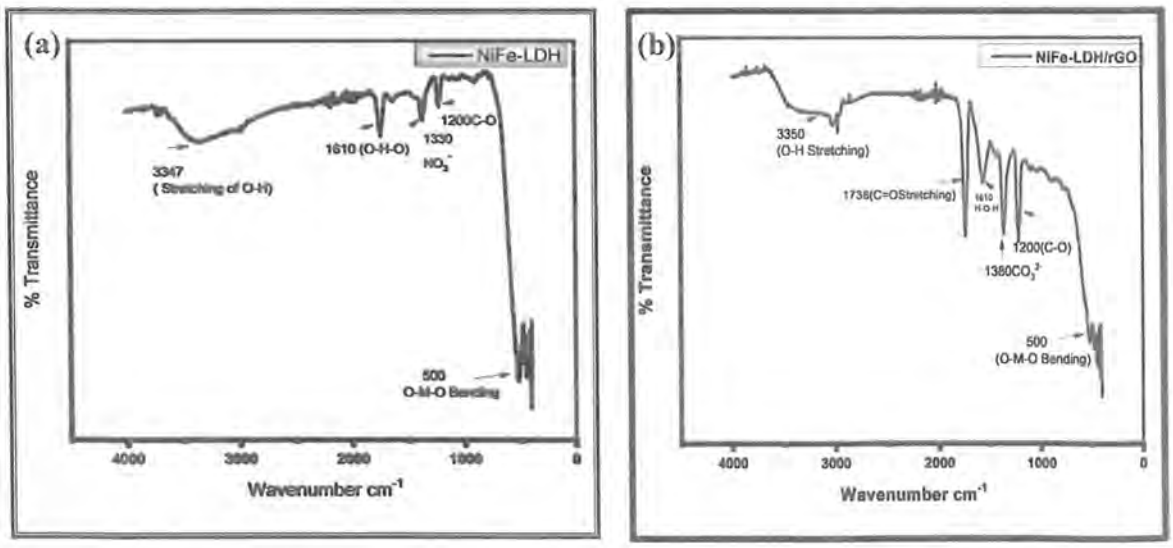

Fig. 3.5 FTIR spectra of (a) NiFe-LDH and (b) NiFe-LDH/rGO.

In both cases, the signals at ≈3350 cm^{-1} can be attributed to the stretching mode of the OH group arising from metal-hydroxyl groups and interlayer H_2O. The bands observed at 1610 cm^{-1} and 1200 cm^{-1} represented the bending vibration of water and C-O vibrations respectively. The peaks at 500 cm^{-1} and below region can be attributed to the M–O–M, M–O, and O–M–O (M=Ni and Fe) vibrations. For NiFe-LDH/rGO interlayered carbonate observed at 1380 cm^{-1}, the vibrations of C=O at 1718 cm^{-1} can be attributed to rGO. While NiFe-LDH exhibited a peak at 1330 cm^{-1} for interlayer nitrate anions.

3.2.2 FTIR analysis of CoFe-LDH and CoFe-LDH/rGO

In the case of the Co-Fe combination of LDH, the FTIR spectra [**Fig. 3.6 (a) and (b)**] contained characteristic peaks for CoFe-LDH and CoFe-LDH/rGO composite. The absorption bands in the region of 3400-3500cm^{-1} represented the stretching mode of O–H and H_2O . The bands at 1600 cm^{-1} represented the bending mode of H_2O

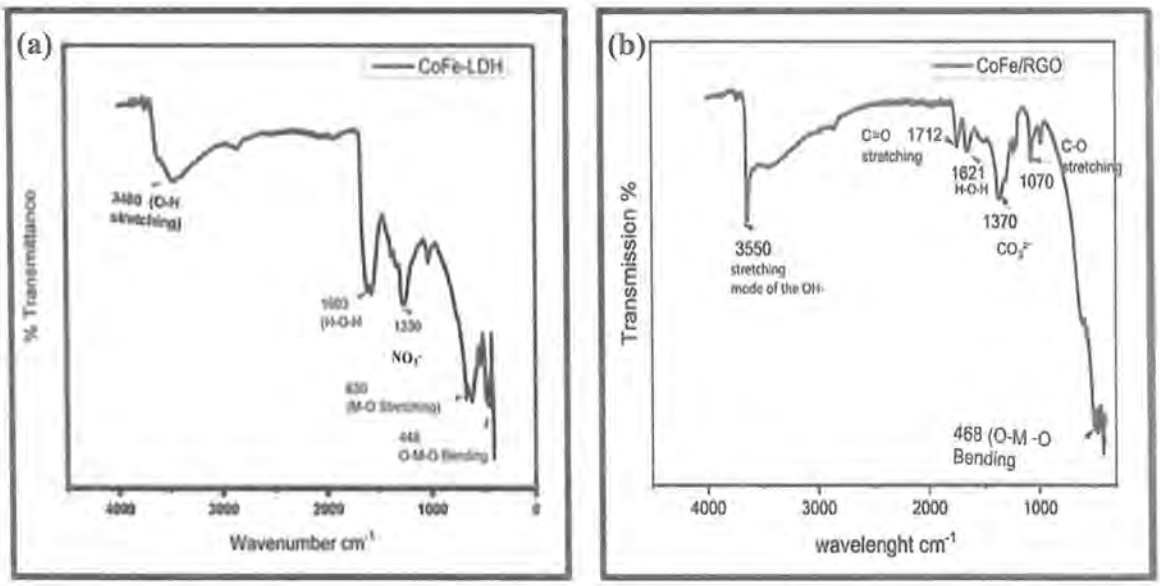

Fig. 3.6 FTIR spectra of (a) CoFe-LDH and (b) CoFe-LDH/rGO.

The peaks in the region below 700 cm^{-1} can be assigned to the M–O–M, M–O, and O–M–O (M=Co and Fe) vibrations. As CoFe-LDH/rGO was interlayered with carbonate anions, so for this the peak was observed at 1370 cm^{-1}, while CoFe-LDH exhibited a peak at 1330 cm^{-1} related to interlayer nitrate anions. For CoFe-LDH/rGO vibrations at 1712 and 1070 cm^{-1} for C=O and C-O respectively, can be attributed to rGO which are missing in CoFe-LDH.

3.2.3 FTIR analysis of NiCo-LDH and NiCo-LDH/rGO

For NiCo-LDH and NiCo-LDH/rGO, the FTIR spectra [**Fig. 3.7 (a) and (b)**] contained characteristic peaks. For both these compounds the absorption peak at 3400 cm^{-1} represented the stretching mode of O–H and H_2O. The bands observed at 1610 cm^{-1} represented the bending vibration of water.

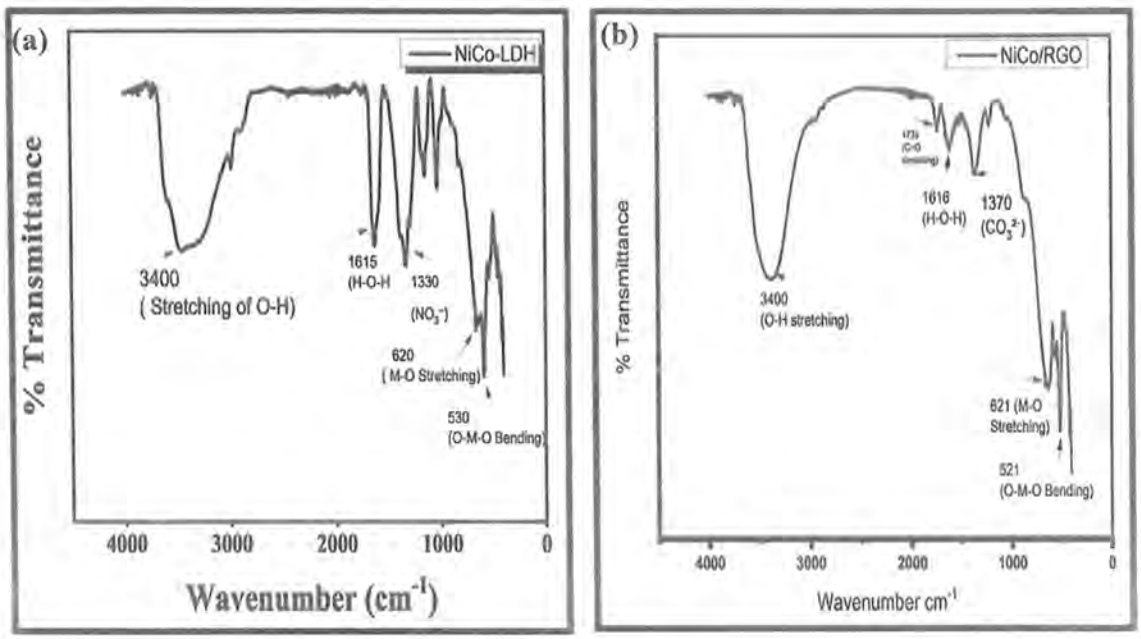

Fig. 3.7 FTIR spectra of (a) NiCo-LDH and (b)NiCo-LDH/rGO.

The peaks in the region below 700 cm^{-1} can be attributed to the M–O–M, M–O, and O–M–O (M=Ni and Co) vibrations. For NiCo-LDH/rGO, the peak was observed at 1380 cm^{-1} for interlayer carbonate anions and the vibrations of C=O at 1735 cm^{-1} can be attributed to rGO. While NiFe-LDH exhibited a peak at 1330 cm^{-1} for interlayer nitrate anions.

From FTIR analysis it is confirmed that the all-synthesized TM-LDHs were intercalated with nitrate anions while their composites were intercalated with carbonate anions. Furthermore, observed vibrations of C=O at 1718 cm^{-1} in FTIR spectra of all synthesized TM-LDH/rGO are related to the presence of rGO. These results of FTIR were matched with previously reported data [110, 115, 116].

3.3 Linear sweep voltametric (LSV) analysis

OER activity of all six synthesized TM-LDHs and TM-LDH/rGO electrocatalysts was investigated by performing LSV in the potential range of 0-1.7 V vs RHE in 1 M KOH solution at a scan rate of 50 mV s^{-1}. The electrode potential of all modified electrodes was measured at a current density of 10 mA cm^{-2} to investigate the OER performance of all synthesized electrocatalysts. As, the η_{10} value serves as a standard reference for evaluating the performance of OER catalysts, as a solar light-assisted hydrogen production system typically operates at a current density range of 10 to 20 mA cm^{-2}. Tafel plots were derived from the corresponding LSV curves by plotting overpotential (η) vs. log j following **equation 3.3**:

$$\eta = a + b \log (j) \qquad (3.3)$$

Where j stands for current density η represents overpotential, and b shows the Tafel slope.

3.3.1 LSV of NiFe-LDH and NiFe-LDH/rGO

GC modified with NiFe-LDH were analyzed through LSV as shown in **Fig. 3.8.** The onset potential was noted to be 1.38 V. The electrode potential was measured as 1.5 V generating an overpotential of 270 mV to achieve the current density of 10 mA cm^{-2}. Tafel plot was used to evaluate the reaction kinetics of the electrocatalyst.

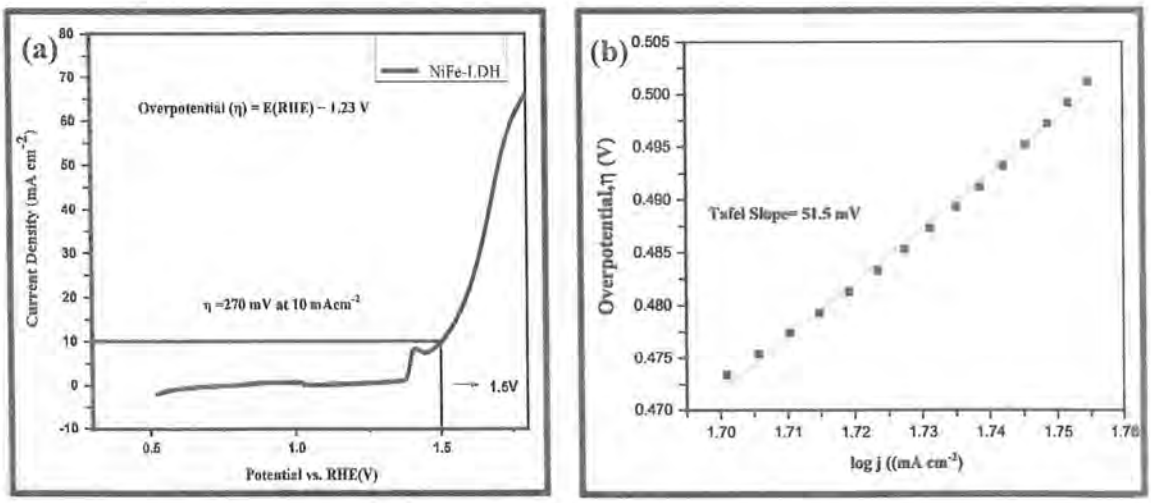

Fig. 3.8 (a) LSV analysis of GCE modified with NiFe-LDH at scan rate of 50 mV s^{-1} in 1 M KOH solution, (b) Tafel plot.

The Tafel slope was calculated 51.5 mV dec^{-1} by plotting overpotential (η) vs. log j. The low value of the Tafel slope shows that a lower potential is required to generate significant current density, reflecting better OER kinetics.

GC modified with NiFe-LDH/rGO was analyzed through LSV (**Fig. 3.9**). The onset potential was noted to be 1.31 V. The electrode potential was measured as 1.49 V showing an over potential of 260 mV to achieve the current density of 10 mA cm^{-2}. The Tafel slope was obtained 46.4 mV dec^{-1} indicating a fast electron transfer reaction.

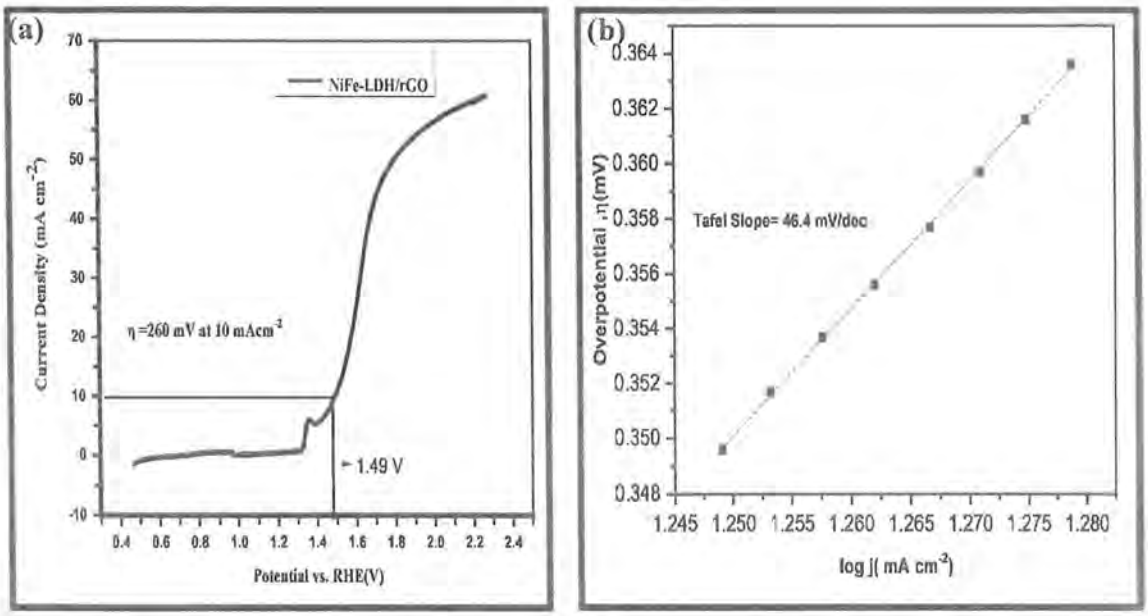

Fig. 3.9 (a) LSV analysis of GCE modified with NiFe-LDH/rGO composite at scan rate of 50 mV s^{-1} in 1 M KOH solution, (b) Tafel plot.

3.3.2 LSV of CoFe-LDH and CoFe-LDH/rGO

LSV curve GC modified with CoFe-LDH (**Fig. 3.10**) indicated that the onset potential was 0.7 V. The value of the electrode potential was 1.56 V showing an over potential of 260 mV to achieve the current density of 10 mA cm^{-2}. Tafel slope was obtained 80.6 mV dec^{-1}.

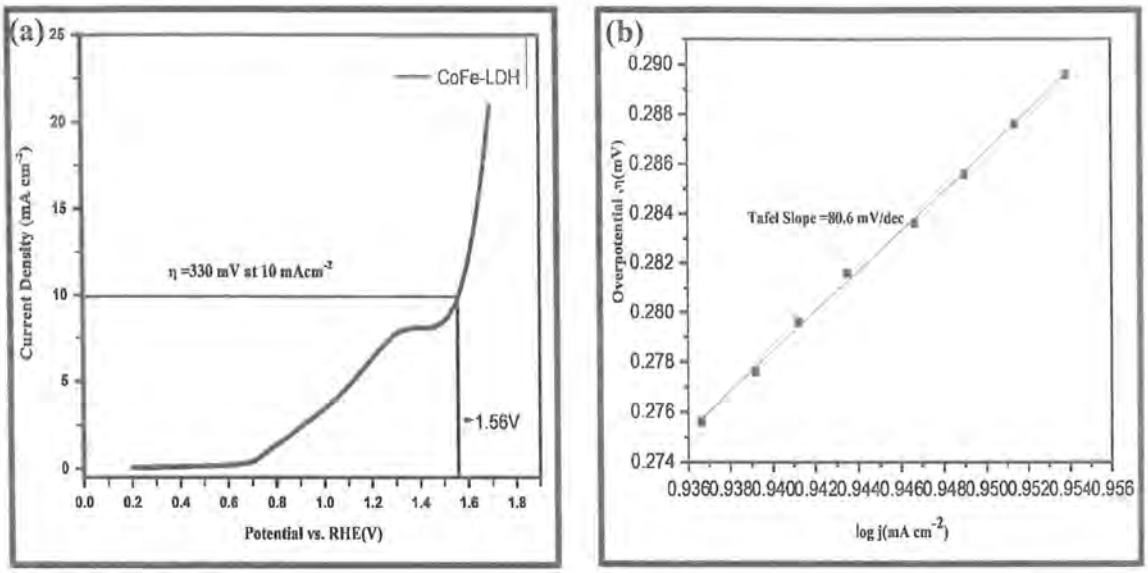

Fig. 3.10 (a) LSV analysis of GCE modified with CoFe-LDH material at scan rate of 50 mV s^{-1} in 1 M KOH solution, (b) Tafel plot.

GC modified with CoFe-LDH/rGO was analyzed through LSV (**Fig. 3.11**). The onset potential was noted to be 0.6 V. The electrode potential was measured as 1.54 V showing an over potential of 310 mV to achieve the current density of 10 mA cm^{-2}. Tafel slope was obtained 53.4 mV dec^{-1} indicating a fast electron transfer reaction.

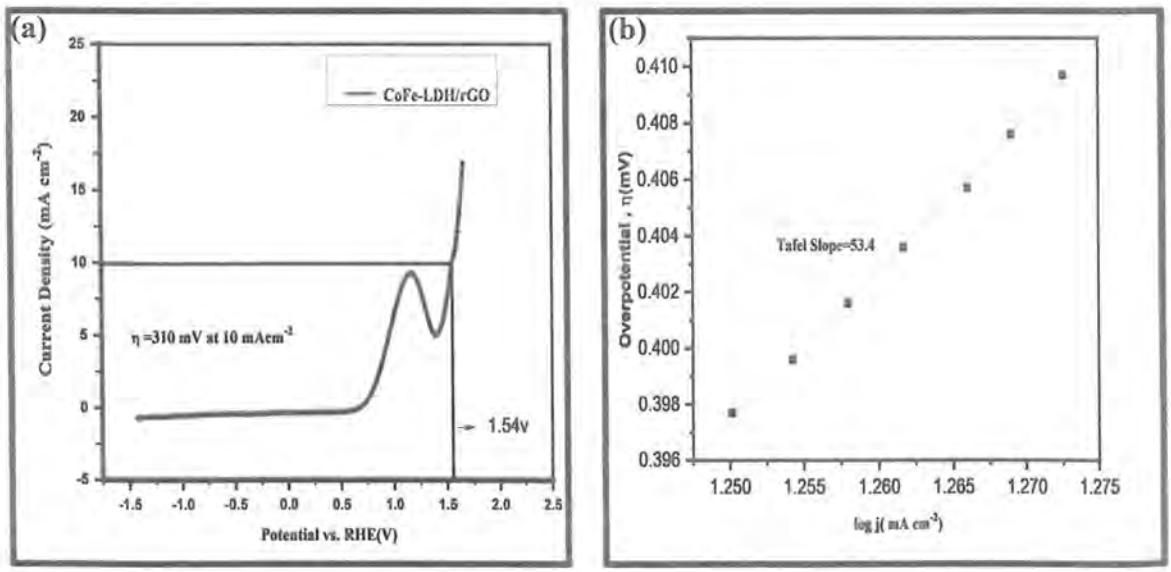

Fig. 3.11 (a) LSV analysis of GCE modified with CoFe-LDH/rGO composite at scan rate of 50 mV s^{-1} in 1 M KOH solution, (b) Tafel plot.

3.3.3 LSV of NiCo-LDH and NiCo-LDH/rGO

Recorded LSV scan for GC electrode modified with NiCo-LDH (**Fig 3.12**) showed on set potential about 0.93 V. In this case, the electrode potential was noted to be 1.52 V giving rise to an overpotential of 390 mV. The calculated value of the Tafel slope was 77 mV dec^{-1}.

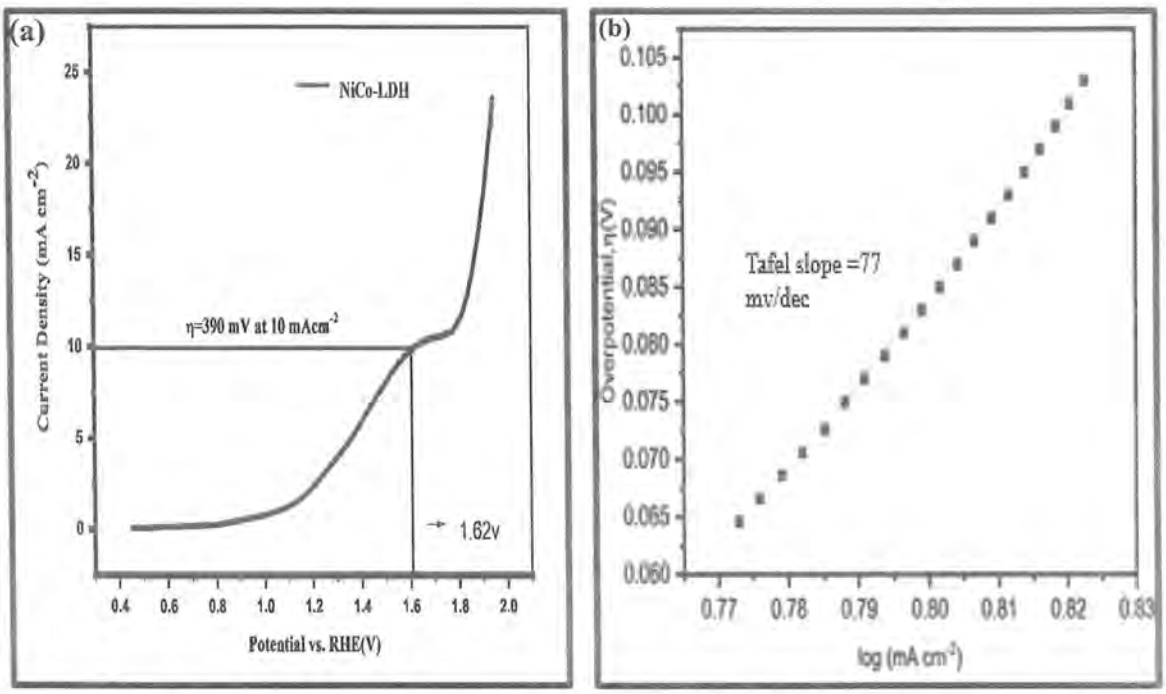

Fig. 3.12 (a)LSV analysis of GCE modified with NiCo-LDH material at scan rate of 50 mV s^{-1} in 1 M KOH solution, (b) Tafel plot.

GC modified with NiCo-LDH/rGO were also analyzed through LSV (**Fig. 3.13**). The onset potential was noted to be 0.89 V. The electrode potential was measured as 1.55 V showing an over potential of 320 mV to achieve the current density of 10 mA cm^{-2}. Tafel slope was obtained 72 mV dec^{-1} indicating a fast electron transfer reaction.

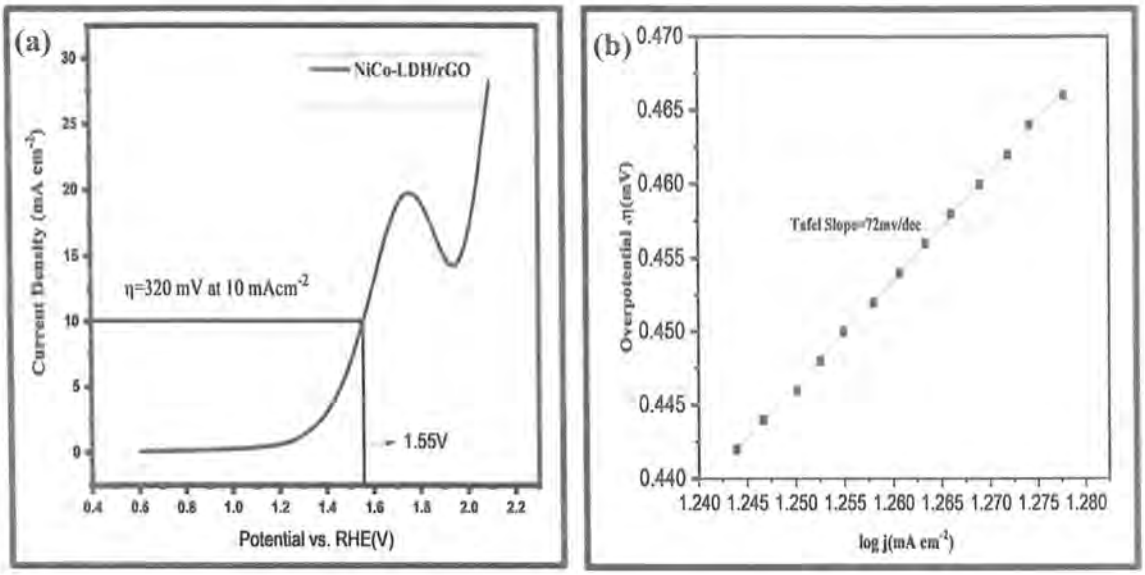

Fig. 3.13 (a)LSV analysis of GCE modified with NiCo-LDH material at scan rate of 50 mV s^{-1} in 1 M KOH solution, (b) Tafel plot.

3.3.4 Comparative LSV analysis of all synthesized material

To examine the OER activities of all synthesized LDH materials, LSV was performed in 1M KOH. The overpotential of 270 mV, 260 mV, 330 mV, 310 mV, 390 mV and 320 mV were required for NiFe-LDH, NiFe-LDH/rGO, CoFe-LDH, CoFe-LDH/rGO, NiCo-LDH and NiCo-LDH/rGO respectively, to attain the current density of 10 mA cm^{-2}. The overpotential for NiFe-LDH/rGO was 260 mV, much lower than the approximately 370 mV required for highly active ruthenium oxide OER electrocatalyst.

Tafel slope values for all synthesized catalysts, were obtained as 51.5 mV dec^{-1}, 46.4 mV dec^{-1}, 80.6 mV dec^{-1}, 53.4 mV dec^{-1} , 77 mV dec^{-1} and 72 mV dec^{-1} for NiFe-LDH, NiFe-LDH/rGO, CoFe-LDH , CoFe-LDH/rGO , NiCo-LDH and NiCo-LDH/rGO, respectively. It is obvious from **Table 3.2** that all these electrocatalysts have shown good OER activity and, the NiFe-LDH/rGO composite displayed an outstanding OER performance by having the lowest Tafel slop and over potential values. It is also observed that the Ni-Fe combination of LDH exhibited the best OER performance as compared to other combinations [(Co-Fe) and (Ni-Co)]. Furthermore, the OER activities of composites of TM-LDHs with rGO have been increased with a smaller Tafel slope and overpotential values as compared to pristine TM-LDHs due to synergistic effects of both these components, indicating facile electron transfer for water oxidation. Based on these

findings, we can conclude that TM-LDH/rGO has not only increased the activity of active site but also exposed additional active sites with the help of rGO suggesting easy electron transport for water oxidation in comparison to pristine LDH materials.

Table 3.2: OER parameters for all synthesized electrocatalysts.

Material	Onset (V)	Tafel slope ($mV\ dec^{-1}$)	η @ 10 $mA\ cm^{-2}$ (mV)
NiFe-LDH	1.38	51.5	270
NiFe-LDH/rGO	1.31	46.4	260
CoFe-LDH	0.7	80.6	330
CoFe-LDH/rGO	0.6	53.4	310
NiCo-LDH	0.93	77	390
NiCo-LDH/rGO	0.89	72	320

3.4 Cyclic voltametric (CV) analysis

Cyclic voltametric analysis of synthesized materials was done to investigate their electrochemical behavior in selected potential ranges. For this purpose, first of all bare GC electrode was scanned at a scan rate of 50 mV s^{-1} in the desired potential range of 0 V to 1.7 V vs. RHE in 1 M KOH. There was no anodic or cathodic peak observed as shown in **Fig. 3.14**.

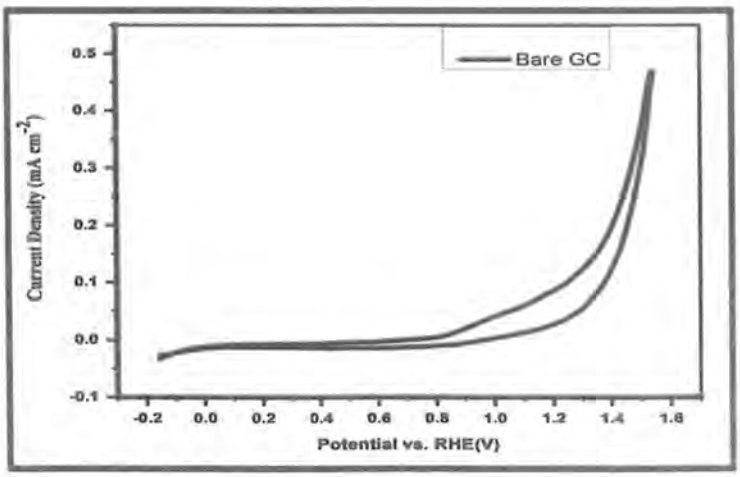

Fig. 3.14 Voltammogram of bare GC at scan rate of 50 mV s^{-1} in 1M KOH solution.

3.4.1 CV analysis NiFe-LDH and NiFe-LDH/rGO

GC electrodes modified with NiFe-LDH and NiFe-LDH/rGO were analyzed in 1M KOH and potential was scanned at 50 mV s^{-1}. A pair of characteristic redox peaks was observed as shown in **Fig. 3.15.**

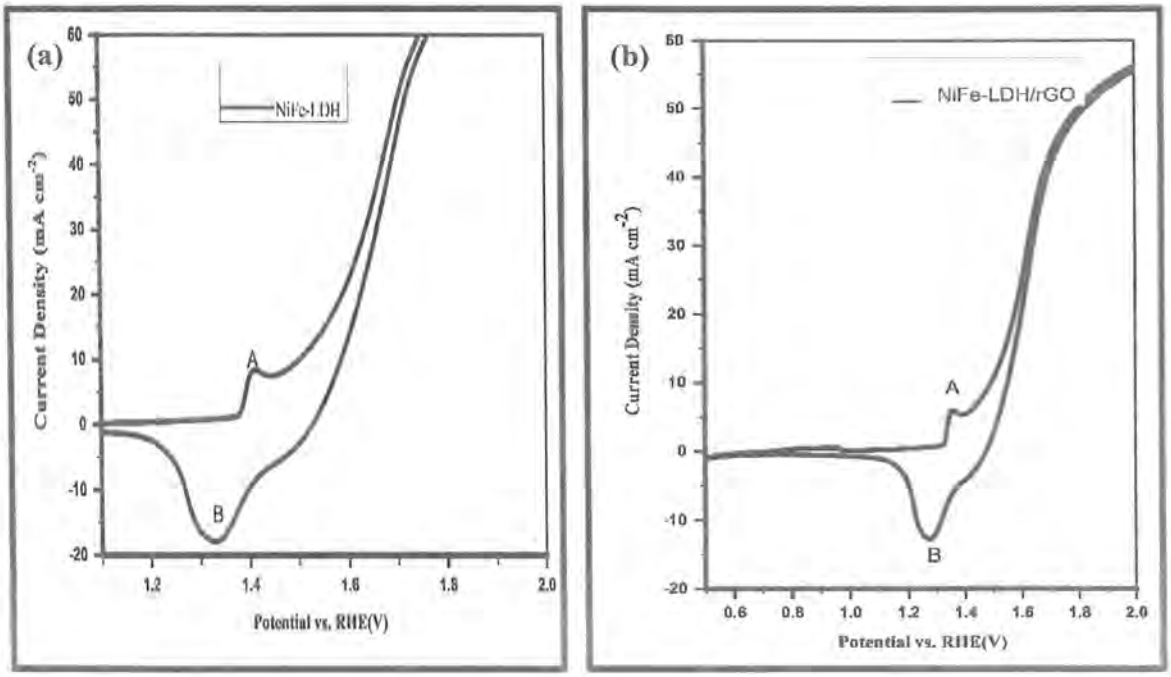

Fig. 3.15 Voltammograms of GC electrode modified with(a) NiFe-LDH material, (b) NiFe-LDH/RGO composite at a scan rate of 50mV s^{-1} in 1 M KOH solution.

An anodic peak appeared at around 1.43 V (A) due to the oxidation of Ni(II) to Ni(III), which overlaps with the onset of OER and with the corresponding reduction peak at 1.35 V V_{RHE} (B) for NiFe-LDH **[Fig. 3.15 (a)]** . CV voltammogram of NiFe-LDH/rGO showed that these characteristic peaks had shifted to lower voltage values depicting the enhanced electrochemical behavior and facilitating the overall process due to the synergistic effect of rGO **[Fig. 3.15 (b)]**. Overlay of both voltammograms of GC modified with NiFe-LDH and NiFe-LDH/rGO is shown in **Fig. 3.16.**

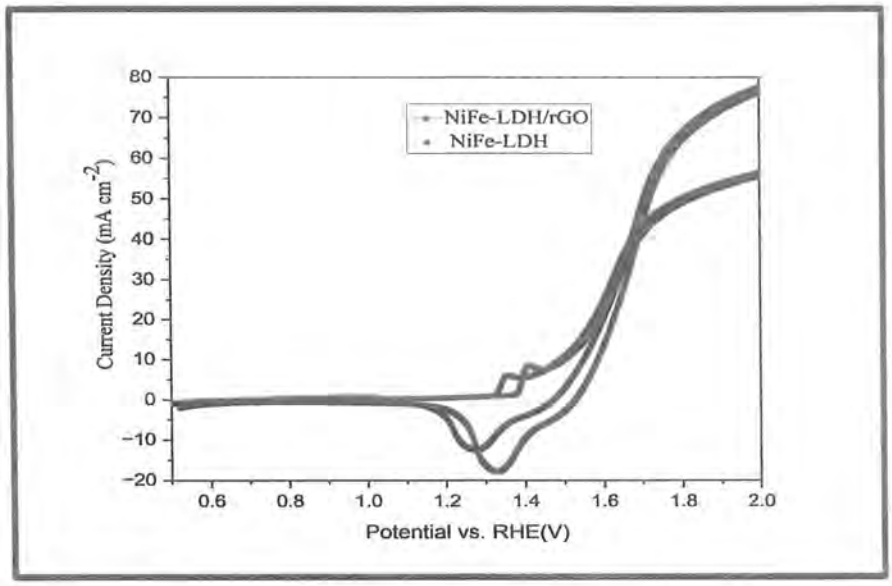

Fig. 3.16 Overlay of both voltammograms of GC modified with NiFe-LDH and NiFe-LDH/rGO.

3.4.2 CV analysis of CoFe-LDH and CoFe-LDH/rGO

GC electrodes modified with CoFe-LDH and CoFe-LDH/rGO were analyzed in 1M KOH and at 50 mV s^{-1} scan rate (**Fig. 3.17**).

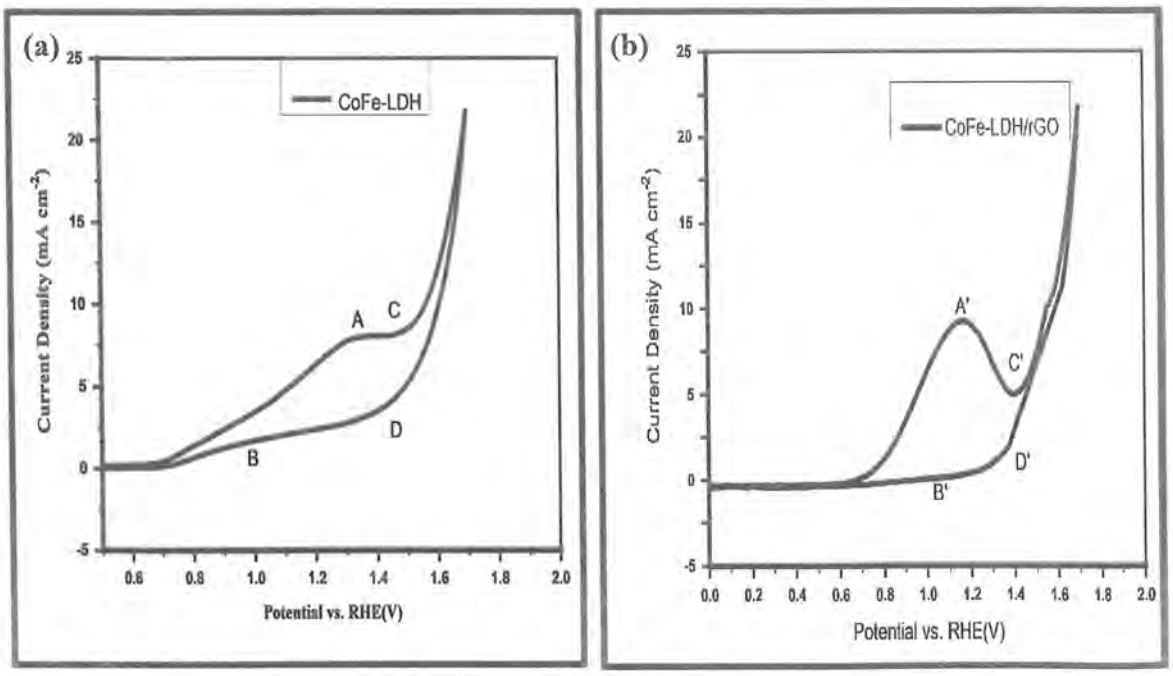

Fig. 3.17 Voltammograms of GC electrode modified with (a) CoFe-LDH material (b) CoFe-LDH/rGO composite at a scan rate of 50 mV s^{-1} in 1 M KOH solution.

The primary oxidation peak at +1.35 V_{RHE} (labeled as A) is observed before the OER activity, moving towards higher anodic potential, a secondary and minor oxidation feature at approximately + 1.55 V_{RHE} (labeled as C) for CoFe-LDH coincides with the onset of the OER. The broad peaks, B at +1.1 V_{RHE} and D at +1.4 V_{RHE} correspond to the respective reduction events on the cathodic scan **[Fig. 3.17 (a)]**. CV scan of CoFe-LDH/rGO has shown a peak shift toward lower potential for this redox reaction **[Fig. 3.17 (b)]**. The overlay of both voltammograms of GC modified with CoFe-LDH and CoFe-LDH/rGO is shown in **Fig. 3.18**.

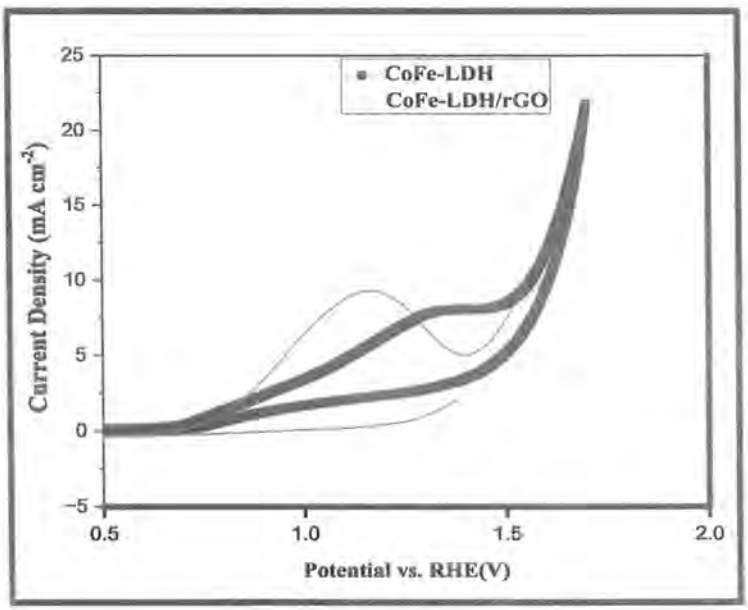

Fig. 3.18 Overlay of both voltammograms of GC modified with CoFe-LDH and CoFe-LDH/rGO.

2.2.3 CV analysis of NiCo-LDH and NiCo-LDH/rGO

GC electrodes modified with NiCo-LDH and NiCo-LDH/rGO were analyzed in 1M KOH and potential was scanned at 50 mV s^{-1} . A broad oxidation peak appeared at around 1.53 V_{RHE} for NiCo-LDH ,as both Ni and Co are part of the LDH structure as shown in **Fig. 3.19.** The back scans revealed a broad cathodic peak suggesting deoxidation of the oxidized species. The Overlay of both voltammograms of GC modified with NiCo-LDH and NiCo-LDH/rGO is shown in **Fig. 3.20**.

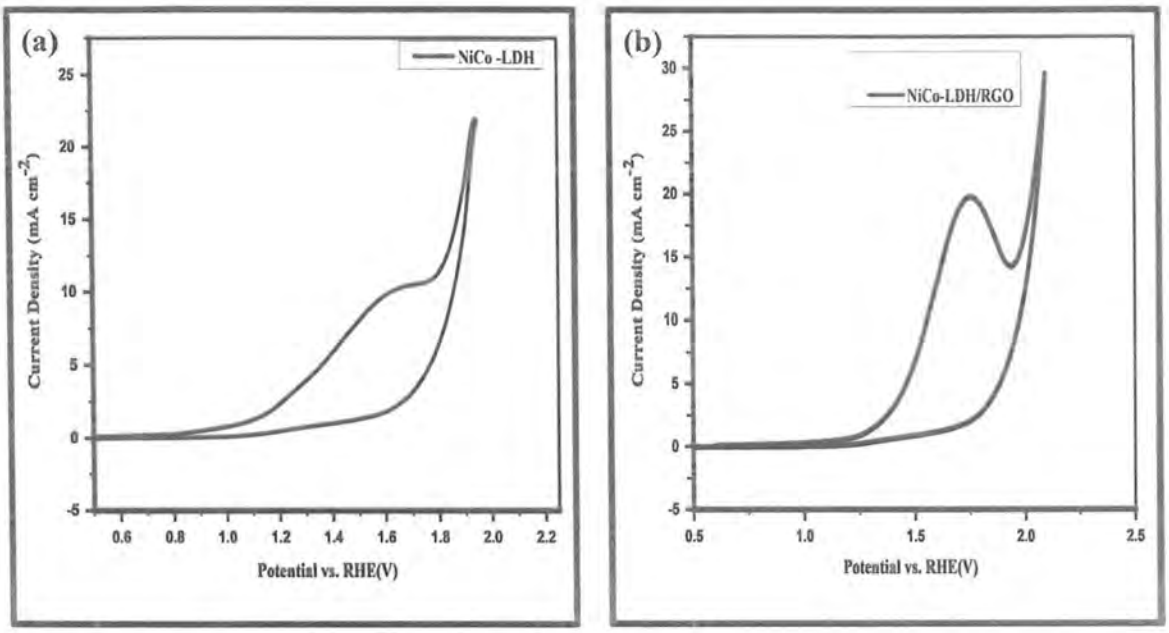

Fig. 3.19 Voltammograms of GC electrode modified with (a) NiCo-LDH material (b) NiCo-LDH/rGO composite at a scan rate of 50 mV s^{-1} in 1 M KOH solution.

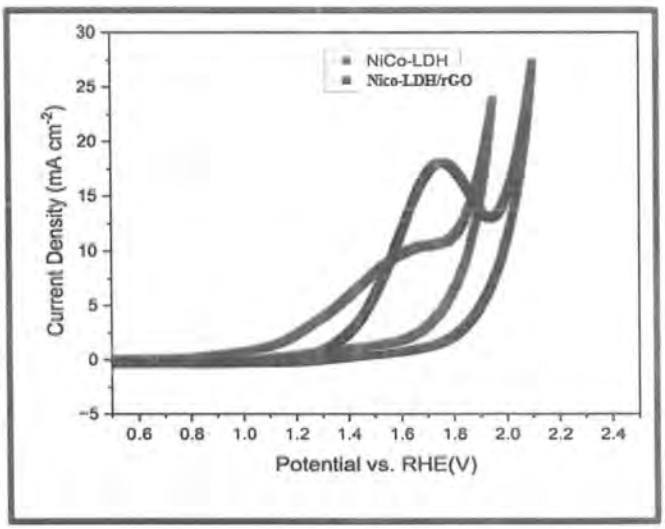

Fig. 3.20 Overlay of both voltammograms of GC modified with NiCo-LDH and NiCo-LDH/rGO.

3.5 Electrochemical impedance spectroscopy (EIS)

Charge transfer properties of all synthesized electrocatalysts were analyzed via impedance measurements in 1M KOH with an AC voltage of 10 mV in the frequency range

of 0.1 to 10^5 Hz. The corresponding Nyquist plots is shown in **Fig. 3.21**. For better visibility, the zoom-in portion of these Nyquist plots is shown in **Figure 3.22(a).**

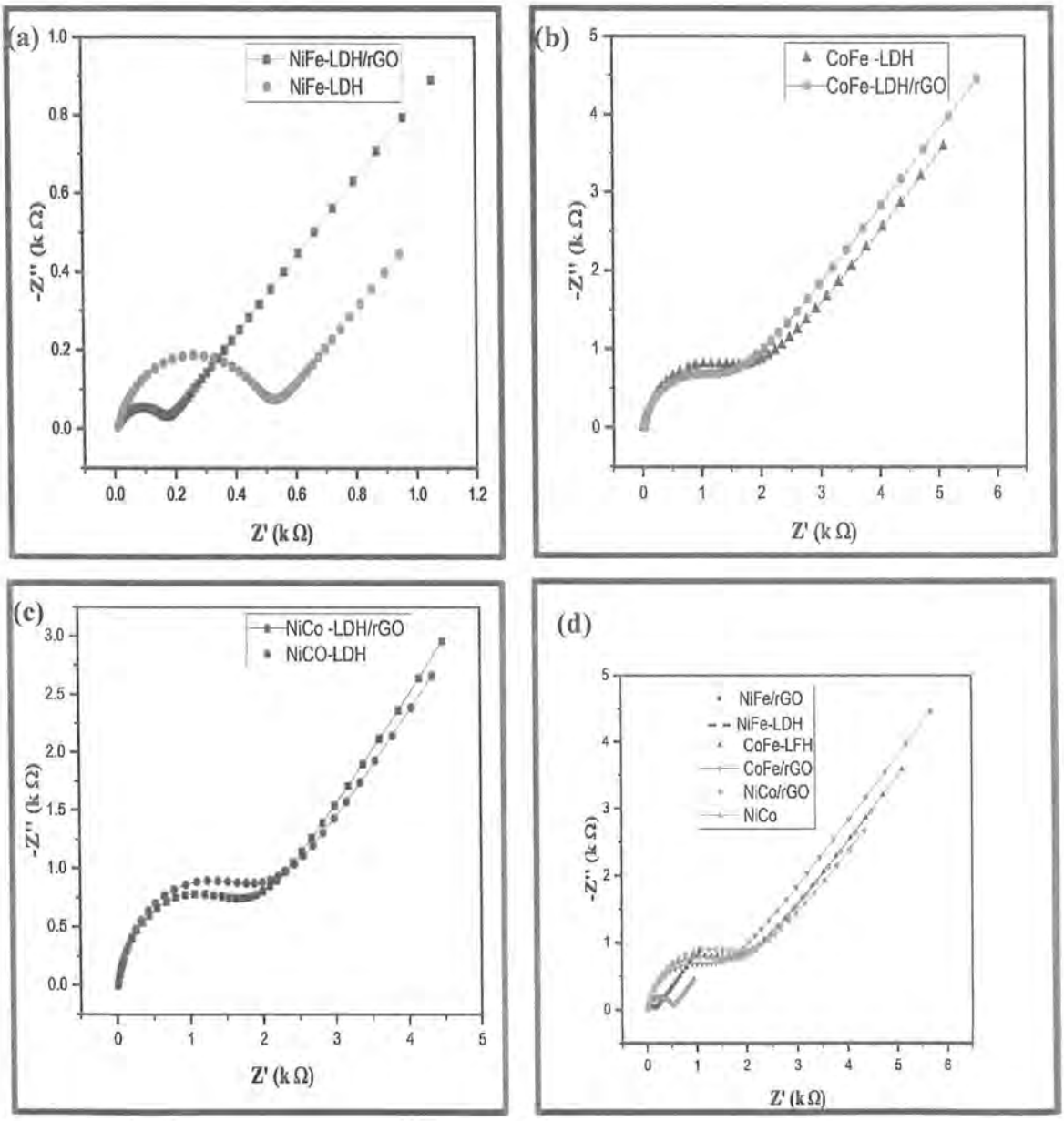

Fig. 3.21 Nyquist plots for (a) NiFe-LDH and NiFe-LDH/rGO, (b) CoFe-LDH and CoFe-LDH/rGO, (c) NiCo-LDH/rGO and NiCo-LDH/rGO (d) Overlay of Nyquist plots for all catalysts in 1 M KOH in the frequency range of 0.1 to 10^5 Hz.

The solution resistance (Rs), charge transfer resistance (Rct) Warburg (W) and double layer capacitance (C_{dl}) for all six electrocatalysts were calculated using Nyquist plots and their equivalent EIS circuit **[Fig. 3.22 (b)]** as given in **Table 3.3.**

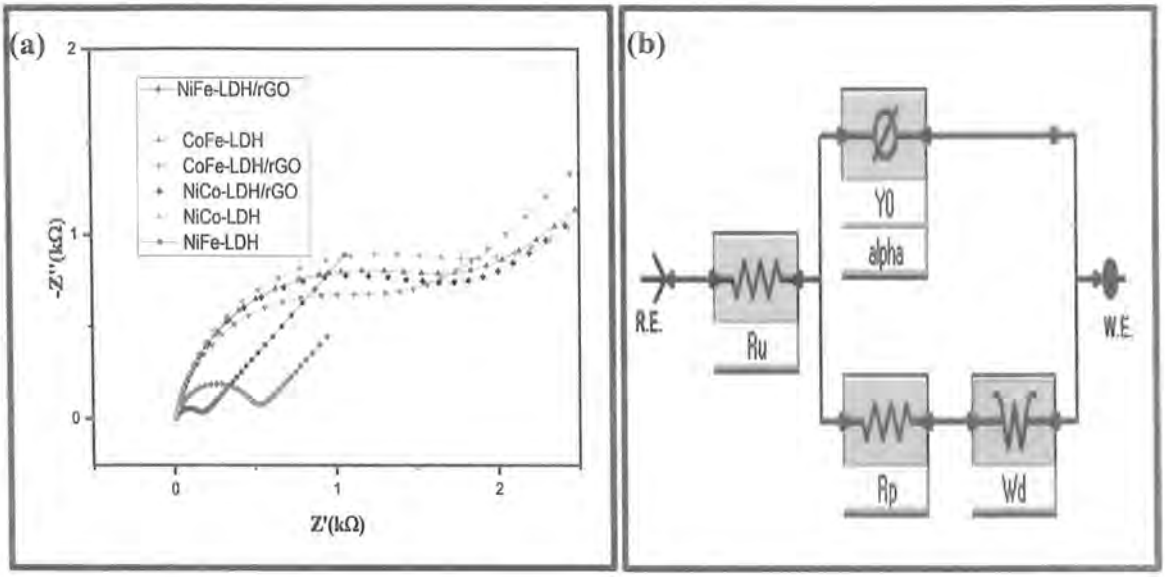

Fig. 3.22 (a) Zoom in portion of all Nyquist plots for clear visibility of semicircular portion. (b) Equivalent EIS circuit.

Table 3.3: EIS parameters of synthesized LDH-based materials.

Material	R_{CT} (kΩ)	Rs (Ω)	C_{dl} (μF)	W (μΩ)
NiFe-LDH	0.49	8.7	2	1768
NiFe-LDH/rGO	0.15	8.4	3	1000
CoFe-LDH	1.61	8.8	4	2502
CoFe-LDH/rGO	1.35	8.5	5	200
NiCo-LDH	1.86	8.9	7	342
NiCo-LDH/rGO	1.65	8.6	9	304

From collected EIS data it was observed that the NiFe-LDH/rGO displayed lowest R_{CT} value among synthesized catalysts, which was about 0.15 kΩ, exhibiting the highest charge transfer efficiency and NiFe-LDH also showed less charge transfer resistance (0.49kΩ). Whereas the R_{CT} value of 1.86 kΩ was measured for NiCo-LDH showing the least charge transfer efficiency among synthesized catalysts. EIS parameters for CoFe-LDH, CoFe-LDH/rGO and NiCo-LDH/rGO lie in between these two extremes.

Conclusions

This study was designed to develop a cost-efficient and highly effective electrocatalyst for the OER using a simple and affordable chemical synthesis method. NiFe-LDH, NiCo-LDH, and CoFe-LDH, were synthesized by the hydrothermal process using hexamethylenetetramine (HMT) as a hydrolysis agent resulting in the formation of TM-LDHs having nitrate anions in their interlayer gallery. While TM-LDH/rGO composites like NiFe-LDH/rGO, CoFe-LDH/rGO, and NiCo-LDH/rGO were prepared via hydrothermal scheme using urea as hydrolysis agent resulting in intercalation of carbonate anions in interlayer space of LDH composite. The XRD analysis revealed the successful formation of well-defined layered structures with high crystallinity. FTIR spectra of synthesized materials exhibited characteristic peaks related to these LDH family and indicate the presence of nitrate group in the interlayer space of pristine TM-LDHs and carbonate group in interlayer gallery TM-LDG/rGO composite. Furthermore, the characteristic bands related to the functional group of rGO indicated the presence of rGO in the composite. Electrochemical analysis (LSV, CV and EIS) was conducted to assess the OER catalytic activity of these TM-LDH and TM-LDH/rGO in an alkaline medium of pH 13.8. OER tests were conducted, and the performance was assessed based on overpotential at a current density of 10 mA cm^{-2} and Tafel slope. The results showed that in the Ni-Fe combination, the order of performance decline is as follows: NiFe-LDH/rGO (260 mV, 46.4 mV dec^{-1}) > NiFe-LDH (270 mV, 51.5 mV dec^{-1}). In the Co-Fe combination, the decline is as follows: CoFe-LDH/rGO (310 mV, 53.4 mV dec^{-1}) > CoFe-LDH (330 mV, 80.6 mV dec^{-1}). For the Ni-Co combination of LDH, the order of performance decline is as follows: NiCo-LDH/rGO (320 mV, 77 mV dec^{-1}) > NiCo-LDH (390 mV, 77 mV dec^{-1}). All the synthesized materials demonstrated good response for OER as overpotential value ranges from 260-390 mV. Moreover, the catalytic activity of LDH composite with rGO has increased as compared to the pristine LDH material. Among all the synthesized materials, NiFe-LDH/rGO exhibited the best OER activity with lowest η of 260 mV and the lowest Tafel slope i.e., 46.4 mV dec^{-1}. Moreover, NiFe-LDH/rGO have shown the least charge transfer resistance (R_{CT}) value of 0.15 kΩ. The obtained results suggest that these TM-LDHs can serve as promising OER active electrocatalysts. However, some aspects of these TM-LDHs need to be further investigated.

References

1. Ali, A.; Long, F.; Shen, P. K., Innovative strategies for overall water splitting using nanostructured transition metal electrocatalysts. *Electrochem. Energy Rev.* **2022,** *5*, 1.
2. Chen, Z.; Wei, W.; Ni, B.-J., Cost-effective catalysts for renewable hydrogen production via electrochemical water splitting: Recent advances. *Curr. Opin. Green Sustain. Chem.* **2021,** *27*, 100398.
3. Sahoo, D. P.; Das, K. K.; Mansingh, S.; Sultana, S.; Parida, K., Recent progress in first row transition metal Layered double hydroxide (LDH) based electrocatalysts towards water splitting: A review with insights on synthesis. *Coord Chem Rev.* **2022,** *469*, 214666.
4. Matsumoto, Y.; Sato, E., Electrocatalytic properties of transition metal oxides for oxygen evolution reaction. *Mater. Chem. Phys.* **1986,** *14*, 397-426.
5. Yu, Z. Y.; Duan, Y.; Feng, X. Y.; Yu, X.; Gao, M. R.; Yu, S. H., Clean and affordable hydrogen fuel from alkaline water splitting: past, recent progress, and future prospects. *Advd Mater.* **2021,** *33*, 2007100
6. Zhang, L.; Zhao, H.; Xu, S.; Liu, Q.; Li, T.; Luo, Y.; Gao, S.; Shi, X.; Asiri, A. M.; Sun, X., Recent advances in 1D electrospun nanocatalysts for electrochemical water splitting. *Small Structures* **2021,** *2*, 2000048.
7. Khan, M. A.; Zhao, H.; Zou, W.; Chen, Z.; Cao, W.; Fang, J.; Xu, J.; Zhang, L.; Zhang, J., Recent progresses in electrocatalysts for water electrolysis. *Electrochem. Energy Rev.* **2018,** *1*, 483-530.
8. Ghosh, S.; Basu, R. N., Multifunctional nanostructured electrocatalysts for energy conversion and storage: current status and perspectives. *Nanoscale* **2018,** *10*, 11241-11280.
9. Rajeshwar, K.; McConnell, R.; Harrison, K.; Licht, S., Renewable energy and the hydrogen economy. *Solar Hydrogen Generation: Toward a Renewable Energy Future* **2008**, *5*, 1-18.
10. Man, I. C.; Su, H. Y.; Calle-Vallejo, F.; Hansen, H. A.; Martínez, J. I.; Inoglu, N. G.; Kitchin, J.; Jaramillo, T. F.; Nørskov, J. K.; Rossmeisl, J., Universality in oxygen evolution electrocatalysis on oxide surfaces. *ChemCatChem* **2011,** *3*, 1159-1165.

11. Zou, X.; Zhang, Y., Noble metal-free hydrogen evolution catalysts for water splitting. *Chem Soc Rev.* **2015,** *44*, 5148-5180.

12. Strmcnik, D.; Uchimura, M.; Wang, C.; Subbaraman, R.; Danilovic, N.; Van Der Vliet, D.; Paulikas, A. P.; Stamenkovic, V. R.; Markovic, N. M., Improving the hydrogen oxidation reaction rate by promotion of hydroxyl adsorption. *Nat. Chem.* **2013,** *5*, 300-306.

13. Santos, D. M.; Sequeira, C. A.; Figueiredo, J. L., Hydrogen production by alkaline water electrolysis. *Quím. Nova* **2013,** *36*, 1176-1193.

14. Zhang, L.; Fan, Q.; Li, K.; Zhang, S.; Ma, X., First-row transition metal oxide oxygen evolution electrocatalysts: regulation strategies and mechanistic understandings. *Sustain. Energy Fuels* **2020,** *4*, 5417-5432.

15. Zeng, K.; Zhang, D., Recent progress in alkaline water electrolysis for hydrogen production and applications. *Prog. Energy Combust. Sci* **2010,** *36*, 307-326.

16. Xia, X.; Deng, N.; Cui, G.; Xie, J.; Shi, X.; Zhao, Y.; Wang, Q.; Wang, W.; Tang, B., NIR light induced H_2 evolution by a metal-free photocatalyst. *Chem Comm.* **2015,** *51*, 10899-10902.

17. Raveendran, A.; Chandran, M.; Dhanusuraman, R., A comprehensive review on the electrochemical parameters and recent material development of electrochemical water splitting electrocatalysts. *RSC Adv.* **2023,** *13*, 3843-3876.

18. Kim, S.; Koratkar, N.; Karabacak, T.; Lu, T.-M., Water electrolysis activated by Ru nanorod array electrodes. *Appl. Phys. Lett.* **2006,** *88*, 26-30.

19. Bard, A. J.; Faulkner, L. R.; White, H. S. Electrochemical methods. In *fundamentals and applications*. John Wiley & Sons Ltd, United Kingdom, **2022**; 46-77.

20. Wang, S.; Lu, A.; Zhong, C.-J., Hydrogen production from water electrolysis: role of catalysts. *Nano Converg.* **2021,** *8*, 1-23.

21. McCreery, R. L., Advanced carbon electrode materials for molecular electrochemistry. *Chem. Rev.* **2008,** *108*, 2646-2687.

22. Aijaz, A.; Masa, J.; Rösler, C.; Xia, W.; Weide, P.; Botz, A. J.; Fischer, R. A.; Schuhmann, W.; Muhler, M., Co@Co_3O_4 encapsulated in carbon nanotube-grafted nitrogen-doped carbon polyhedra as an advanced bifunctional oxygen electrode. *Angew. Chem., Int. Ed.* **2016,** *55*, 4087-4091.

23. Wang, P.; Zhang, X.; Zhang, J.; Wan, S.; Guo, S.; Lu, G.; Yao, J.; Huang, X., Precise tuning in platinum-nickel/nickel sulfide interface nanowires for synergistic hydrogen evolution catalysis. *Nat. commun.* **2017,** *8*, 14580.
24. Lee, Y.; Suntivich, J.; May, K. J.; Perry, E. E.; Shao-Horn, Y., Synthesis and activities of rutile IrO_2 and RuO_2 nanoparticles for oxygen evolution in acid and alkaline solutions. *J. Phys. Chem. Lett.* **2012,** *3*, 399-404.
25. Kasian, O.; Grote, J. P.; Geiger, S.; Cherevko, S.; Mayrhofer, K. J., The common intermediates of oxygen evolution and dissolution reactions during water electrolysis on iridium. *Angew. Chem., Int. Ed.* **2018,** *57*, 2488-2491.
26. Zhang, H.; Liu, Y.; Chen, T.; Zhang, J.; Zhang, J.; Lou, X. W., Unveiling the activity origin of electrocatalytic oxygen evolution over isolated Ni atoms supported on a N-doped carbon matrix. *Adv Mater* **2019,** *31*, 1904548.
27. Xue, Z.; Zhang, X.; Qin, J.; Liu, R., Revealing Ni-based layered double hydroxides as high-efficiency electrocatalysts for the oxygen evolution reaction: a DFT study. *J. Mater. Chem. A* **2019,** *7*, 23091-23097.
28. Kötz, R.; Lewerenz, H.; Stucki, S., XPS studies of oxygen evolution on Ru and RuO_2 anodes. *J. Electrochem. Soc.* **1983,** *130*, 825.
29. Lv, L.; Yang, Z.; Chen, K.; Wang, C.; Xiong, Y., 2D layered double hydroxides for oxygen evolution reaction: from fundamental design to application. *Adv. Energy Mater.* **2019,** *9*, 1803358.
30. Li, Y.; Zhang, L.; Peng, J.; Zhang, W.; Peng, K., Magnetic field enhancing electrocatalysis of Co_3O_4/NF for oxygen evolution reaction. *J. Power Sources* **2019,** *433*, 226704.
31. Peña, M. A.; Fierro, J., Chemical structures and performance of perovskite oxides. *Chem. Rev.* **2001,** *101*, 1981-2018.
32. Bockris, J. O. M.; Otagawa, T., The electrocatalysis of oxygen evolution on perovskites. *J. Electrochem. Soc.* **1984,** *131*, 290.
33. Smith, R. D.; Prévot, M. S.; Fagan, R. D.; Trudel, S.; Berlinguette, C. P., Water oxidation catalysis: electrocatalytic response to metal stoichiometry in amorphous metal oxide films containing iron, cobalt, and nickel. *J. Am. Chem. Soc.* **2013,** *135*, 11580-11586.

34. Wang, X.; Kolen'ko, Y. V.; Bao, X. Q.; Kovnir, K.; Liu, L., One-step synthesis of self-supported nickel phosphide nanosheet array cathodes for efficient electrocatalytic hydrogen generation. *Angew. Chem.* **2015,** *127*, 8306-8310.

35. Xiao, P.; Sk, M. A.; Thia, L.; Ge, X.; Lim, R. J.; Wang, J.-Y.; Lim, K. H.; Wang, X., Molybdenum phosphide as an efficient electrocatalyst for the hydrogen evolution reaction. *Energy Environ. Sci.* **2014,** *7*, 2624-2629.

36. Liu, P.; Rodriguez, J. A., Catalysts for hydrogen evolution from the [NiFe] hydrogenase to the Ni_2P (001) surface: the importance of ensemble effect. *J. Am. Chem. Soc.* **2005,** *127*, 14871-14878.

37. Jiang, N.; You, B.; Sheng, M.; Sun, Y., Electrodeposited cobalt-phosphorous-derived films as competent bifunctional catalysts for overall water splitting. *Angew. Chem.* **2015,** *127*, 6349-6352.

38. Chen, B.; Li, R.; Ma, G.; Gou, X.; Zhu, Y.; Xia, Y., Cobalt sulfide/N, S codoped porous carbon core–shell nanocomposites as superior bifunctional electrocatalysts for oxygen reduction and evolution reactions. *Nanoscale* **2015,** *7*, 20674-20684.

39. Zhu, L.; Susac, D.; Teo, M.; Wong, K.; Wong, P.; Parsons, R.; Bizzotto, D.; Mitchell, K.; Campbell, S., Investigation of CoS_2-based thin films as model catalysts for the oxygen reduction reaction. *J. Catal.* **2008,** *258*, 235-242.

40. Bini, M.; Monteforte, F., Layered double hydroxides (LDHs): versatile and powerful hosts for different applications. *J. Anal. Pharm. Res* **2018,** *7*, 00206.

41. Li, T.; Miras, H. N.; Song, Y.-F., Polyoxometalate (POM)-layered double hydroxides (LDH) composite materials: design and catalytic applications. *Catalysts* **2017,** *7*, 260.

42. Caia, Z.; Wanga, P.; Yanga, J.; Wanga, X., Update on recent designing strategies of transition metal-based layered double hydroxides bifunctional electrocatalysts. *ES Energy Environ.* **2019,** *5*, 22-36.

43. Anantharaj, S.; Karthick, K.; Kundu, S., Evolution of layered double hydroxides (LDH) as high performance water oxidation electrocatalysts: A review with insights on structure, activity and mechanism. *Mater. Today Energy* **2017,** *6*, 1-26.

44. Chowdhury, P. R.; Medhi, H.; Bhattacharyya, K. G.; Hussain, C. M., Recent progress in the design and functionalization strategies of transition metal-based layered double

hydroxides for enhanced oxygen evolution reaction: A critical review. *Coord Chem Rev.* **2023,** *483*, 215083

45. Gong, M.; Dai, H., A mini review of NiFe-based materials as highly active oxygen evolution reaction electrocatalysts. Nano Res **2014**, *8*, 23-39.
46. Fan, K.; Chen, H.; Ji, Y.; Huang, H.; Claesson, P. M.; Daniel, Q.; Philippe, B.; Rensmo, H.; Li, F.; Luo, Y., Nickel–vanadium monolayer double hydroxide for efficient electrochemical water oxidation. *Nat.Commun* **2016,** *7*, 11981.
47. Eftekhari, A., Materials today energy. *Mater. Today* **2017,** *5*, 37-57.
48. Tyndall, D.; Craig, M. J.; Gannon, L.; McGuinness, C.; McEvoy, N.; Roy, A.; García-Melchor, M.; Browne, M. P.; Nicolosi, V., Demonstrating the source of inherent instability in NiFe LDH-based OER electrocatalysts. *J. Mater Chem. A* **2023,** *11*, 4067-4077.
49. Suen, N.-T.; Hung, S.-F.; Quan, Q.; Zhang, N.; Xu, Y.-J.; Chen, H. M., Electrocatalysis for the oxygen evolution reaction: recent development and future perspectives. *Chem Soc Rev.* **2017,** *46*, 337-365.
50. Tahir, M.; Pan, L.; Idrees, F.; Zhang, X.; Wang, L.; Zou, J.-J.; Wang, Z. L., Electrocatalytic oxygen evolution reaction for energy conversion and storage: A comprehensive review. *Nano Energy* **2017,** *37*, 136-157
51. Ma, W.; Ma, R.; Wang, C.; Liang, J.; Liu, X.; Zhou, K.; Sasaki, T., A Superlattice of Alternately Stacked Ni–Fe Hydroxide Nanosheets and Graphene for Efficient Splitting of Water. *ACS Nano* **2015,** *9*, 1977-1984.
52. Wang, Z.; Long, X.; Yang, S., Effects of Metal Combinations on the Electrocatalytic Properties of Transition-Metal-Based Layered Double Hydroxides for Water Oxidation: A Perspective with Insights. *ACS Omega* **2018,** *3*, 16529-16541.
53. Friebel, D.; Louie, M. W.; Bajdich, M.; Sanwald, K. E.; Cai, Y.; Wise, A. M.; Cheng, M.-J.; Sokaras, D.; Weng, T.-C.; Alonso-Mori, R.; Davis, R. C.; Bargar, J. R.; Nørskov, J. K.; Nilsson, A.; Bell, A. T., Identification of Highly Active Fe Sites in (Ni,Fe)OOH for Electrocatalytic Water Splitting. *J. Am. Chem Soc.* **2015,** *137*, 1305-1313

54. Trotochaud, L.;Young, S. L.; Ranney, J. K.; Boettcher, S.W., Nickel–iron oxyhydroxide oxygen-evolution electrocatalysts: the role of intentional and incidental iron incorporation. *J. Am Chem Soc.* **2014,** *136*, 6744-6753.

55. Tyndall, D.; Jaskaniec, S.; Shortall, B.; Roy, A.; Gannon, L.; O'Neill, K.; Browne, M. P.; Coelho, J.; McGuinness, C.; Duesberg, G. S., Postsynthetic treatment of nickel–iron layered double hydroxides for the optimum catalysis of the oxygen evolution reaction. *NPJ 2D Mater. Appl.* **2021,** *5*, 73.

56. Zhou, Y.; Hu, J.; Yang, L.; Gao, Q., Recent advances of two-dimensional CoFe layered-double-hydroxides for electrocatalytic water oxidation. *Chin Chem Lett* **2022,** *33*, 2845-2855.

57. Feng, L.; Li, A.; Li, Y.; Liu, J.; Wang, L.; Huang, L.; Wang, Y.; Ge, X., A highly active CoFe layered double hydroxide for water splitting. *ChemPlusChem* **2017,** *82*, 483-488.

58. Hung, S.-F.; Chan, Y.-T.; Chang, C.-C.; Tsai, M.-K.; Liao, Y.-F.; Hiraoka, N.; Hsu, C.-S.; Chen, H. M., Identification of Stabilizing High-Valent Active Sites by Operando High-Energy Resolution Fluorescence-Detected X-ray Absorption Spectroscopy for High-Efficiency Water Oxidation. *J. Am Chem Soc* **2018,** *140*, 17263-17270.

59. Xu, M.; Wei, M., Layered double hydroxide-based catalysts: recent advances in preparation, structure, and applications. *Adv. Funct. Mater.* **2018,** *28*, 1802943.

60. Dionigi, F.; Zeng, Z.; Sinev, I.; Merzdorf, T.; Deshpande, S.; Lopez, M. B.; Kunze, S.; Zegkinoglou, I.; Sarodnik, H.; Fan, D., In-situ structure and catalytic mechanism of NiFe and CoFe layered double hydroxides during oxygen evolution. *Nat. Commun.* **2020,** *11*, 2522.

61. Wang, M.; Liu, X.; Liu, H.; Zhao, D.; Wu, X., NiCo layered double hydroxide nanosheets with enhanced electrochemical performance. *J. Alloys Compd.* **2022,** *903*, 163926.

62. Sun, H.; Miao, Y.; Wu, T.; Wang, Q., Exfoliation of bimetallic (Ni, Co) carbonate hydroxide nanowires by Ar plasma for enhanced oxygen evolution. *Chem Comm.* **2020,** *56*, 872-875.

63. Zhao, Y.; Wang, Q.; Bian, T.; Yu, H.; Fan, H.; Zhou, C.; Wu, L.-Z.; Tung, C.-H.; O'Hare, D.; Zhang, T., Ni^{3+} doped monolayer layered double hydroxide nanosheets as efficient electrodes for supercapacitors. *Nanoscale* **2015,** *7*, 7168-7173.

64. Jiang, J.; Zhang, A.; Li, L.; Ai, L., Nickel–cobalt layered double hydroxide nanosheets as high-performance electrocatalyst for oxygen evolution reaction. *J. Power Sources* **2015,** *278*, 445-451.

65. Wang, H.; Sun, F.; Qi, J.; Zhang, D.; Sun, H.; Wang, Q.; Li, Z.; Wu, Y. A.; Hu, Z.; Wang, B., Recent progress on layered double hydroxides: Comprehensive regulation for enhanced oxygen evolution reaction. *Mater. Today Energy* **2022,** *27*, 101036.

66. Cai, Z.; Bu, X.; Wang, P.; Ho, J. C.; Yang, J.; Wang, X., Recent advances in layered double hydroxide electrocatalysts for the oxygen evolution reaction. *J. Mater. Chem. A* **2019,** *7*, 5069-5089.

67. Yi, H.; Liu, S.; Lai, C.; Zeng, G.; Li, M.; Liu, X.; Li, B.; Huo, X.; Qin, L.; Li, L., Recent advance of transition-metal-based layered double hydroxide nanosheets: synthesis, properties, modification, and electrocatalytic applications. *Adv. Energy Mater.* **2021,** *11*, 2002863.

68. Das, S.; Dash, S. K.; Parida, K., Kinetics, isotherm, and thermodynamic study for ultrafast adsorption of azo dye by an efficient sorbent: ternary Mg/(Al+ Fe) layered double hydroxides. *ACS omega* **2018,** *3*, 2532-2545.

69. Nayak, S.; Mohapatra, L.; Parida, K., Visible light-driven novel gC 3 N 4/NiFe-LDH composite photocatalyst with enhanced photocatalytic activity towards water oxidation and reduction reaction. *J. Mater Chem. A* **2015,** *3*, 18622-18635.

70. Malak-Polaczyk, A.; Vix-Guterl, C.; Frackowiak, E., Carbon/layered double hydroxide (LDH) composites for supercapacitor application. *Energy & fuels* **2010,** *24*, 3346-3351.

71. Liu, L.; Cheng, M.; Yang, Z., Improved performance of flower-like ZnAl LDH growing on carbon nanotubes used in zinc–nickel secondary battery. *Electrochim. Acta* **2018,** *277*, 67-76.

72. Ribeiro, L. N.; Alcântara, A. C.; Darder, M.; Aranda, P.; Araújo-Moreira, F. M.; Ruiz-Hitzky, E., Pectin-coated chitosan–LDH bionanocomposite beads as potential systems for colon-targeted drug delivery. *Int. J. Pharma.* **2014,** *463*, 1-9.

73. Khan, M. A.; Fattah-alhosseini, A.; Kaseem, M., Recent advances in the design and surface modification of titanium-based LDH for photocatalytic applications. *Inorg Chem Commun* **2023,** *153*, 110739.

74. Daneshvar, H.; Dorraji, M. S.; Amani-Ghadim, A.; Rasoulifard, M., Enhanced sonocatalytic performance of ZnTi nano-layered double hydroxide by substitution of Cu (II) cations. *Ultrason. Sonochem.* **2019,** *58*, 104632.

75. Cavani, F.; Trifiro, F.; Vaccari, A., Hydrotalcite-type anionic clays: Preparation, properties and applications. *Catal. Today* **1991,** *11*, 173-301.

76. Ferrari, I. V., A top-to-bottom overview of the main Applications of 2D green nanomaterial: Layered Double Hydroxides (LDHs) in recent years. *Electrochim. Acta* **2023**, *2*, 1-27.

77. Jin, W.; Ha, S.; Myung, J.-H.; Kim, B. C.; Park, D.-H., Ceramic layered double hydroxide nanohybrids for therapeutic applications. *J. Korean Ceram. Soc.* **2020,** *57*, 597-607.

78. Yang, Q.-Z.; Chang, Y.-Y.; Zhao, H.-Z., Preparation and antibacterial activity of lysozyme and layered double hydroxide nanocomposites. *Water Res.* **2013,** *47*, 6712-6718.

79. Cao, L.; Cao, Y.; Liu, X.; Luo, Q.; Liu, W.; Zhang, W.; Mou, X.; Yao, T.; Wei, S., Coupling confinement activating cobalt oxide ultra-small clusters for high-turnover oxygen evolution electrocatalysis. *J. Mater Chem. A* **2018,** *6*, 15684-15689.

80. Benck, J. D.; Hellstern, T. R.; Kibsgaard, J.; Chakthranont, P.; Jaramillo, T. F., Catalyzing the hydrogen evolution reaction (HER) with molybdenum sulfide nanomaterials. *ACS Catal.* **2014,** *4*, 3957-3971.

81. Li, Y.; Bao, X.; Chen, D.; Wang, Z.; Dewangan, N.; Li, M.; Xu, Z.; Wang, J.; Kawi, S.; Zhong, Q., A Minireview on Nickel-Based Heterogeneous Electrocatalysts for Water Splitting. *ChemCatChem* **2019,** *11*, 5913-5928.

82. Youn, D. H.; Park, Y. B.; Kim, J. Y.; Magesh, G.; Jang, Y. J.; Lee, J. S., One-pot synthesis of NiFe layered double hydroxide/reduced graphene oxide composite as an

efficient electrocatalyst for electrochemical and photoelectrochemical water oxidation. *J. Power Sources* **2015,** *294*, 437-443.

83. Perrozzi, F.; Prezioso, S.; Ottaviano, L., Graphene oxide: from fundamentals to applications. *J. Phys: Condens. Matter* **2014,** *27*, 013002.
84. Marchezi, P. E.; Sonai, G. G.; Hirata, M. K.; Schiavon, M. A.; Nogueira, A. F., Understanding the role of reduced graphene oxide in the electrolyte of dye-sensitized solar cells. *J. Phys Chem C* **2016,** *120*, 23368-23376.
85. Long, X.; Li, J.; Xiao, S.; Yan, K.; Wang, Z.; Chen, H.; Yang, S., A strongly coupled graphene and FeNi double hydroxide hybrid as an excellent electrocatalyst for the oxygen evolution reaction. *Angew. Chem., Int. Ed.* **2014,** *53*, 7584-7588.
86. Allou, N. g. B.; Saikia, P.; Borah, A.; Goswamee, R. L., Hybrid nanocomposites of layered double hydroxides: an update of their biological applications and future prospects. *Colloid Polym. Sci.* **2017,** *295*, 725-747.
87. Zhao, J.; Wang, X.-r.; Chen, F.-w.; He, C.; Wang, X.-j.; Li, Y.-p.; Liu, R.-h.; Chen, X.-m.; Hao, Y.-j.; Yang, M., A one-step synthesis of hierarchical porous CoFe-layered double hydroxide nanosheets with optimized composition for enhanced oxygen evolution electrocatalysis. *Inorg. Chem. Front.* **2020,** *7*, 737-745.
88. Okamoto, K.; Iyi, N.; Sasaki, T., Factors affecting the crystal size of the MgAl-LDH (layered double hydroxide) prepared by using ammonia-releasing reagents. *Appl. Clay Sci.* **2007,** *37*, 23-31.
89. Wan, H.; Liu, J.; Ruan, Y.; Lv, L.; Peng, L.; Ji, X.; Miao, L.; Jiang, J., Hierarchical configuration of $NiCo_2S_4$ nanotube@Ni–Mn layered double hydroxide arrays/three-dimensional graphene sponge as electrode materials for high-capacitance supercapacitors. *ACS Appl Mater Interfaces* **2015,** *7*, 15840-15847.
90. Chen, H.; Hu, L.; Chen, M.; Yan, Y.; Wu, L., Nickel–cobalt layered double hydroxide nanosheets for high-performance supercapacitor electrode materials. *Adv Funct. Mater.* **2014,** *24*, 934-942.
91. Lu, Z.; Xu, W.; Zhu, W.; Yang, Q.; Lei, X.; Liu, J.; Li, Y.; Sun, X.; Duan, X., Three-dimensional NiFe layered double hydroxide film for high-efficiency oxygen evolution reaction. *Chem Comm* **2014,** *50*, 6479-6482.

92. Liu, R.; Wang, Y.; Liu, D.; Zou, Y.;Wang, S., Water-plasma-enabled exfoliation of ultrathin layered double hydroxide nanosheets with multivacancies for water oxidation. *Adv Mater.* **2017,** *29*, 1701546.

93. Gualandi, I.; Monti, M.; Scavetta, E.; Tonelli, D.; Prevot, V.; Mousty, C., Electrodeposition of layered double hydroxides on platinum: insights into the reactions sequence. *Electrochim. Acta* **2015,** *152*, 75-83.

94. Yang, M.; Cheng, H.; Gu, Y.; Sun, Z.; Hu, J.; Cao, L.; Lv, F.; Li, M.; Wang, W.; Wang, Z., Facile electrodeposition of 3D concentration-gradient Ni-Co hydroxide nanostructures on nickel foam as high performance electrodes for asymmetric supercapacitors. *Nano Research* **2015,** *8*, 2744-2754.

95. Yu, X.; Zhang, M.; Yuan, W.; Shi, G., A high-performance three-dimensional Ni–Fe layered double hydroxide/graphene electrode for water oxidation. *J. Mater Chem. A* **2015,** *3*, 6921-6928.

96. Han, X.; Yu, C.; Yang, J.; Zhao, C.; Huang, H.; Liu, Z.; Ajayan, P. M.; Qiu, J., Mass and charge transfer coenhanced oxygen evolution behaviors in CoFe-layered double hydroxide assembled on graphene. *Adv. Mater. Interfaces* **2016,** *3*, 1500782.

97. Yang, F.; Sliozberg, K.; Sinev, I.; Antoni, H.; Bähr, A.; Ollegott, K.; Xia, W.; Masa, J.; Grünert, W.; Cuenya, B. R., Synergistic effect of cobalt and iron in layered double hydroxide catalysts for the oxygen evolution reaction. *ChemSusChem* **2017,** *10*, 156-165.

98. Wang, Q.; Shang, L.; Shi, R.; Zhang, X.; Zhao, Y.; Waterhouse, G. I.; Wu, L. Z.; Tung, C. H.; Zhang, T., NiFe layered double hydroxide nanoparticles on Co, N-codoped carbon nanoframes as efficient bifunctional catalysts for rechargeable zinc–air batteries. *Adv. Energy Mater.* **2017,** *7*, 1700467.

99. Liu, W.; Bao, J.; Guan, M.; Zhao, Y.; Lian, J.; Qiu, J.; Xu, L.; Huang, Y.; Qian, J.; Li, H., Nickel–cobalt-layered double hydroxide nanosheet arrays on Ni foam as a bifunctional electrocatalyst for overall water splitting. *Dalton trans.* **2017,** *46*, 8372-8376.

100. Yang, Y. J.; Duan, M.; Yan, C.; Zhao, D.; Jiang, C.; Duan, X.; Song, X., Facile synthesis of CoFe-LDH/MWCNT/rGO nanocomposite as efficient bifunctional electrocatalysts for oxygen evolution and reduction. *J. Electroanal. Chem.* **2020,** *856*, 113697.

110. Qu, J.; Li, F.; Wang, M.; Subakti, S.; Deconinck, M.; Chen, G.; Li, Y.; Liu, L.; Wang, X.; Yu, M., One-Pot Synthesis of Nitrate-Intercalated NiFe Layered Double Hydroxides with an 8.2 Å Interlayer Spacing. *Adv Mater Interfaces* **2022,** *9*, 2200973.

111. Iyi, N.; Matsumoto, T.; Kaneko, Y.; Kitamura, K., A novel synthetic route to layered double hydroxides using hexamethylenetetramine. *Chem. Lett.* **2004,** *33*, 1122-1123.

112. Gayathri, S.; Arunkumar, P.; Kim, J.; Han, J. H., Bimetallic Layered Hydroxide Nitrate@ Graphene Oxide as an Electrocatalyst for Efficient Non-Enzymatic Glucose Sensors: Tuning Sensitivity by Hydroxide-Regulated $M_2(OH)_{4-n}(A^{n-})$ Phases Derived from Solvent Engineering. *ACS Sustain. Chem. Eng.* **2022,** *10*, 1689-1701.

113. Lu, Y.; Yang, P.; Li, Y.; Wen, D.; Luo, J.; Wang, S.; Wu, F.; Fang, L.; Pang, Y., A facile synthesis of NiFe-layered double hydroxide and mixed metal oxide with excellent microwave absorption properties. *Molecules* **2021,** *26*, 5046.

114. Jin, W.; Liu, F.; Guo, X.; Zhang, J.; Zheng, L.; Hu, Y.; Mao, J.; Liu, H.; Xue, Y.; Tang, C., Self-supported CoFe LDH/$Co_{0.85}Se$ nanosheet arrays as efficient electrocatalysts for the oxygen evolution reaction. *Catal. Sci. Technol* **2019,** *9*, 5736-5744.

115. Li, R.; Hu, Z.; Shao, X.; Cheng, P.; Li, S.; Yu, W.; Lin, W.; Yuan, D., Large scale synthesis of NiCo layered double hydroxides for superior asymmetric electrochemical capacitor. *Sci. Rep.* **2016,** *6*, 18737.

116. Tian, M.; Liu, C.; Neale, Z. G.; Zheng, J.; Long, D.; Cao, G., Chemically bonding NiFe-LDH nanosheets on rGO for superior lithium-ion capacitors. *ACS Appl Mater Interfaces* **2019,** *11*, 35977-35986.